HEMODYNAMIC DESIGN OPTIMIZATION OF A

VENTRICULAR CANNULA:

EVALUATION AND IMPLEMENTATION OF OBJECTIVE

FUNCTIONS

by

Samuel J. Hund

Bachelors of Science in Engineering, University of Colorado, 1999

Masters of Science in Engineering, University of Colorado, 2001

Submitted to the Graduate Faculty of

the School of Engineering in partial fulfillment

of the requirements for the degree of

Master of Science

University of Pittsburgh

2006

UNIVERSITY OF PITTSBURGH

SCHOOL OF ENGINEERING

This thesis was presented

by

Samuel J. Hund

It was defended on

March 8th, 2006

and approved by

James F. Antaki, PhD, Department of Bioengineering and Department of Surgery

Harvey S. Borovetz, PhD, Department of Bioengineering and Department of Surgery

Anne M. Robertson, PhD, Department of Mechanical Engineering

Thesis Advisor: James F. Antaki, PhD, Bioengineering

HEMODYNAMIC DESIGN OPTIMIZATION OF A VENTRICULAR CANNULA:

EVALUATION AND IMPLEMENTATION OF OBJECTIVE FUNCTIONS

Samuel J. Hund, M.S.

University of Pittsburgh, 2006

Shape optimization has been used for decades to improve the aerodynamic performance of automobiles and aircraft. The application of this technology to blood-wetted medical devices have been limited, in part, due to the ambiguity of hemodynamic variables associated with biocompatibility – specifically hemolysis, platelet activation, and thrombus formation. This study undertook a systematic evaluation of several objective functions derived directly from the flow field. We specifically focused on the optimization of a two-dimensional blood conduit (cannula) by allowing free variation of the centerline and cross-sectional area. The flow was simulated using computational fluid dynamics (CFD) at a nominal flow rate of 6 lpm and boundary conditions consistent with an abdominally positioned left-ventricular-assist device (LVAD). The objectives were evaluated both locally and globally. The results demonstrated similarities between four of the functions: vorticity, viscous dissipation, principal shear stress, and power-law (PL) blood damage models based on shear history. Of the functions analyzed, those found to be most indicative of flow separation and clearance were *flow deviation index* and the Peclet Number. The conclusions from these studies will be applied to ongoing development of algorithms for optimizing the flow path of rotary blood pumps, cannula, and other blood contacting devices.

TABLE OF CONTENTS

LIST OF TABLES

LIST OF FIGURES

PREFACE

I would like to thank my thesis committee and all of those who helped advise me through the years, include Robert Leben, Greg Burgreen, and Omar Ghattas. I would also like to thank the Sangria Project and its members as well as the NSF Center for e-Design who were invaluable collaborators over the past few years.

1.0   INTRODUCTION AND BACKGROUND

The development of blood-wetted medical devices is very difficult and ill posed. The complex nature of blood makes it difficult to completely simulate the biocompatibility of these devices. Even when a suitable design is found, the results may not scale from one application to the next, necessitating a redesign for each case. Despite these challenges, computer simulations and numerical optimization provide practical and cost-effective methods for the design and evaluation of these devices. The aerospace and automotive industries have used shape optimization (SO) for several decades to improve their products. The biomedical industry has seen an increase in the use computational fluid dynamics (CFD), but it is lagging behind other major industries in its implementation; and has not adopted SO in any meaningfully way. One of the challenges to implementing optimization into the biomedical industry is relating simulation results to biocompatibility or biological performance. For example, Giersiepen (1) developed a power-law model for blood trauma that was based on highly restricted conditions. Investigators have attempted to apply it blindly to CFD analyses, but its validity under generalized conditions has never been validated; hence its utility as a predictive tool is questioned(2, 3). Other simulations of flow-related blood trauma, such as platelet deposition models presented by Sorensen et al. (4, 5), have yet to be expanded to complex flow patterns similar to those found in medical devices. The goal of this thesis is to carry out a systematic analysis of the most commonly used macroscopic models (reduced order) for blood damage to predict microscopic phenomena. Additional models were introduced to fill gaps that were perceived in describing the relevant hemodynamic phenomena for biocompatibility.

The first section describes a detailed study leading to the selection of several key functions representing blood damage, suitable for use as objective functions for blood-wetted medical devices. The second section of this thesis involves applying these functions to a benchmark problem, namely the ventricular cannula for a left ventricular assist device (LVAD),

such as the Streamliner VAD. This benchmark case was chosen for several reasons. Cannulae have generally not been studied to the same extent as other hemodynamic problems – such as end-to-side anastomosis. Of the few studies that have been performed on cannulae, most involve material properties, while very little work has been done on the flow path(6-12). Secondly flow through curved tubes, including cannula, is not trivial. The flow exhibits several interacting phenomena such as separation and Dean Vortices. Finally, the flow profile exiting the cannula can dramatically affect the performance of the VAD to which it is attached. In summary, the study of flow in a cannula strikes a balance between simplicity and non-triviality: the problem is simple enough to be tractable, yet complex enough so that the results are neither trivial nor intuitive, but useful.

This thesis is organized in a logical fashion, beginning with an overview of the basics of blood rheology and trauma. The following introductory sections describe some of the common methods by which CFD is used to estimate blood damage, and introduces optimization in the context of the finite element method (FEM). The Methods sections provides a more detailed description of the specific methods and approaches employed n this study, including the blood damage indicators chosen. The Results section describes the implementation of the objective functions into the design of the cannula. The thesis concludes with a discussion of the results and future work.

1.1   BLOOD DAMAGE

The design goal of any medical device is to maximize **safety** and **efficacy**. In this respect, blood damage is one of the most important issues for blood-wetted devices. Blood damage refers to a physiological and morphological change that occurs to any component of the blood, and can take on several forms. The most traditional analysis of blood damage is *hemolysis*: the rupture of red blood cells. Hemolysis can lead to hemoglobinemia or anemia. A second indicator of blood damage is thrombosis, which is the leading cause of device failure and device related complications (13). A third indicator is shear induced white blood cell and platelet activation, but the underlying physics are similar to those behind hemolysis. It is important to have a basic understanding of blood in order to understand how it is damaged, so a brief summary of blood is

provided in the following section, followed by a detailed discussion of how blood is damaged by surface contact and flow conditions.

1.1.1   Composition and Rheology of Blood

Blood is an important biological fluid and has always had a mystical significance to man (14). Blood is responsible for transporting oxygen, nutrients, and hormones to other tissues in the body. It is also responsible for removing carbon dioxide and other waste products produced by tissues. It is also important in regulating fluid, electrolyte, and pH balances. Finally it is integral in maintaining homeostasis, modulating inflammation, and fighting disease. Blood is a complex mixture of ions, proteins, and formed elements. The formed elements float in a fluid mixture known as plasma, which contains water, proteins, lipids, vitamins, and other compounds. Although, most of the components of the plasma are important in sustaining life, the proteins that are crucial to this discussion are fibrinogen, von Willebrand factor, and various coagulation factors.

There are three divisions of formed elements. The first and most abundant are called Erythrocytes, which are better known as red blood cells (RBCs). The second type known as platelets (Plts), are the formed elements primarily responsible for hemostasis. The third set of formed elements is composed of several different types of cells collectively know as Leukocytes, or white blood cells (WBCs). These relatively large cells are responsible for producing antibodies, destroying bacteria and viruses, and neutralizing toxins. WBCs are also responsible for the inflammatory response. The relative proportion of blood volume comprised of formed elements is approximately 35-50% RBCs, and less than 1% Plts and WBCs (14, 15). The remaining 64-49% is comprised of plasma. The plasma has a density of 1.03 g/cm^3 and that of the RBCs is 1.10 g/cm^3. The density of the slurry is typically 1.05 g/cm^3.

The complex composition of blood is responsible for its non-Newtonian rheological behavior. The formed elements cause the blood to exhibit shear-thinning behavior, meaning its viscosity drops over a range of increasing shear rate. At low strain rates, blood has an *apparent* viscosity of about 135 cP and decreases down to an asymptotic value of about 3.5 cP at around 100 s^{-1} (16). Hematocrit, temperature (17), red blood cell deformability, and protein concentration can drastically change the value of the blood viscosity (18). Blood also shows

some viscoelastic behavior (19), but the most significant signs of this phenomenon require the blood to be motionless for upwards of 10 minutes (20). Sharp et al. and others show that viscoelastic models of blood only show a 2% change in the peak velocity and a 3% change in wall shear stress when viscoelastic models were employed for flow in a tube (21). This was illustrated by a study of Mann et al. who showed that a solutions separan and xantham gum, which exhibits viscoelastic and shear-thinning behavior, approximated the shear stress profiles of blood in an experimental VAD better than a pure Newtonian fluid (22, 23).

1.1.2 Hemolysis

Hemolysis, or blood cell lysis, typically refers to the rupture of the membrane of the red blood cell and liberation of its contents, primarily hemoglobin. Although research of mechanical trauma to blood has been studied for decades, investigation into the microscopic mechanisms of shear induced hemolysis is still in its infancy (24). It is known that red blood cells are resistant to large compressive pressures up 2000 mmHg, but can easily be ruptured by exposure to small shearing forces around 200 mmHg (25-28). There is also a complex shear-exposure relationship, where a red blood cell can survive large stresses (1.5-3000 mmHg) for short periods of time (1, 28). Pressure gradients and fluctuations have been shown to cause hemolysis (29-32). Kuchar and Sutera predicted that flow features that cause hemolysis are turbulence, geometries that produce high-shear stresses, sharp corners, stagnation regions, and flow separation, but Sutera showed that turbulence only increased hemolysis near walls (33, 34).

If a large number of RBCs are destroyed over a short period of time, a lethal level (approximately 160 mg/dL) of hemoglobin can develop in the blood stream causing renal failure and possibly death (35-37). Several steps are required to remove hemoglobin from the free stream (14). First it is picked up by Macrophages, then its iron is stripped and the protein digested. The iron is then bound to a protein called transferrin and is released back into the blood stream where it can be used just like dietary iron (14).

Even if hemolysis is not high enough to cause hemoglobinemia, it may still pose a danger because of anemia. Although not a fatal condition anemia caused by long term blood cell destruction can results in weakness, slower healing, lower exercise tolerance, and a lower quality

of life. Hemolysis is also an indicator of a more dangerous, but less easily detected phenomena of platelet activation, describe below.

1.1.3 Platelet Activation

Platelets activation can be accomplished through several mechanisms. The platelet acts as the first line of defense in blood clotting by activating when contacting a foreign surface, which forms a "plug" when collagen is exposed by damaged tissue. Platelets can also activate when coming into contact with certain chemicals, known as *agonists*, such as adenosine-diphosphate (ADP), thrombin, and Thromboxane A2 (TxA2) (38). Surface and chemical activation of platelets is irreversible and results in the release of agonists, an inversion of the membrane, receptor activation, and other conformal changes. Activated platelets that remain in the blood stream are usually cleared from the circulation in the spleen. Shear stress can also activate platelets directly, but this can be either reversible or irreversible (39). Reversible activation only results in changes in fibrinogen receptor that increases the likelihood of aggregates forming. Activated platelets are also more likely to stick to the surface and other activated platelets. The deleterious consequences of platelet activation in prosthetic blood-wetted devices can be quite catastrophic.

1.1.4 Thrombosis and the Coagulation Cascade

Blood loss can be life threatening, so all of the components necessary to stop bleeding are actively floating through the body in an inert state. If a blood vessel is ruptured exposing the underlying collagen, the body can almost instantaneously start the process to clot through platelet adhesion and the coagulation cascade. Unfortunately, artificial surfaces can activate the same mechanisms, which could lead to device failure or injury to the patients.

Virchow's triad elegantly ties thrombosis to the contacting surface, the blood properties, and the fluid flow. The surface effects and methods of mitigating them are beyond the scope of this work, so only the basic principals will be discussed here. Coagulation involves the activation of platelets and a complex cascade of protein reaction that results in a solid thrombus. Major

flow features that are known to contribute to this process includes recirculation regions, stagnation zones, large eddies, and low bulk rate.

Device related thrombosis starts when plasma proteins adsorb to a foreign surface (40). Thrombin is cleaved from prothrombin through a complex set of protein reactions starting when factor XII adheres to a foreign surface with prekallikrein and high-molecular-weight kinase. Thrombin is responsible for breaking fibrinogen down into fibrin monomers and activating factor XIII. The fibrin monomers self-polymerize into fibrin and are cross-linked into a stable mesh by factor XIIIa.

Device-related thrombosis is a serious cause for concern. First, the cannula or other medical device can be occluded by an excessive amount of thrombus causing interruption of vital flow. Secondly, emboli can break off of a large thrombus formation and lodge in distal tissue cause an infarction. The patient could suffer from stroke, heart attack, or other organ failure (13). Thrombosis is a major cause of device failure in stents (41-46), prosthetic heart valves (47-52), ventricular assist devices (53-55), fistula (56-58), and small diameter vascular grafts (59-62).

1.2   CURRENT METHODS FOR ANALYZING BLOOD DAMAGE

Blood damage can be categorized as hemolysis, platelet activation, and the formation of thrombus. Several methods are commonly used to predict blood damage in medical devices and several others could possibly contribute to it. (See Table 1) It is more convenient to break these functions down into two main categories. The first are those that predict hemolysis or shear induced platelet activation. These functions include vorticity, viscous dissipation, power-law (PL) blood damage models, elongation, shear stress, and acceleration force. The second group contains those that determine areas of recirculation and stagnation, where agonists and activated platelets can build up or where surface adhesion is likely. The functions in this group include confluency (the divergence of flow velocity) stagnation area, residence time, the Peclet Number, and the Damkohler Number. These will be further detailed in subsequent sections.

6

Table 1: List of quantities that can estimate blood damage

Function	Expression	Brief Summary
Vorticity	$$\omega^2$$	Measurement of Local Fluid Rotation
Viscous Dissipation	$$\mu\dot{\gamma}^2$$	Measure of viscous energy loss
Principal Shear Stress	$\tau_{max} = \sqrt{(\tau_{xx} - \tau_{yy})^2/2 + \tau_{xy}}$	Shear stress in the principal frame
Power-Law Damage Model	$$A\tau^\alpha t^\beta$$	Mathematical model fitted to blood damage curves
Acceleration	$$\left(\frac{\vec{a}\cdot\vec{u}}{U}\right)^2$$	Acceleration experienced by a particle following streamlines
Gradient of Acceleration	$$(\nabla a)^2$$	Gradient of previous quantity
Elongation	$\varepsilon^2 = \sum_{i=1}^{N} D_{ii}^2$	Normal rate of strain
Confluency	$\phi^2 = a\tan(\left|\vec{f}\times\vec{u}\right|/_{\vec{f}\cdot\vec{u}})$	Devation of flow from a desired direction
Stagnation Area	$A = (1 - \tanh(\alpha(U - 0.05*\vec{u})))/2$	Area of Low Flow
Residence Time	$$t = h/_U$$	Average time taken for flow to cross an element
Peclet Number	$$Pc = Ud/_D$$	Ratio of convection to diffusion
Damkohler Number	$$Da = kd/_U$$	Ratio of reaction rate to convection

1.2.1 Indices for Estimating Hemolysis

Viscous dissipation and shear stress have typically been linked to blood damage (11, 63, 64). Viscous dissipation is the rate at which kinetic energy is lost due to viscous friction, or the power (stress times strain) lost due to the friction in the flow. It can also be considered a scalar interpretation of the shear stress, since the shear stress is proportional to the strain rate, for a Newtonian fluid.

Most research into hemolysis directly relates it to shear stress (11, 25-28, 63-65). Shear stress is a difficult parameter to examine because it is a tensor quantity. The most common methods for analyzing stress is to calculate the norm of the tensor. The simplest form for two and three-dimensional flow is the product of viscosity and shear rate: $\mu\dot{\gamma}$, or alternatively the maximum principal stress: τ_{max}. Only the maximum principal shear stress will be analyzed, since viscous dissipation is proportional to the square of the first method. Yeleswarapu et al. (66) developed a model for blood damage:

$$\dot{Di} = \left(\frac{\sigma(t)}{\sigma_o}\right)^r \frac{1}{[1-D(t)]^k}.$$

According to this hemolysis model, it is possible to minimize the rate of damage by minimizing the shear stress history.

Vorticity is a measure of circulation and rotation in a fluid, and is twice the average shear rate of a fluid element. Only one group has used vorticity as an objective function for hemolysis (11, 63), but vorticity can indicate boundary layers where there is high shear stresses and turbulence. Vorticity is also prevalent in turbulent flow.

Hemolysis is a complex relationship between shear stress and exposure time. Experiments in simple flow fields have been used to determine typical stress-time exposure relationships for blood. In 1990 Giersiepen fit in-vitro experimental data to a power-law equation using the shear stress, τ, and exposure time, t. He used it to measure both blood damage though hemolysis and the change in LDH, a platelet released agonist. Mitsamura recently refit the parameters because the original model over predicted hemolysis in some devices (67). Boreda et al. developed a *platelet stimulation function* (PSF) using the same model (68, 69). Platelets are presumed to activate when the value of the PSF reaches 1000.

The PL models, summarized in Table 2, are based in the Lagrangian frame of reference. The most common way of evaluating these damage indices (Di) is to integrate the value over the streamline, using one of the following forms:

$$Di = \int_T A\beta\tau^\alpha t^{\beta-1} dt$$

$$Di = \int_T A\beta\tau^\alpha t^{\beta-1} dt + \int_\tau A\alpha\tau^{\alpha-1} t^\beta d\tau.$$

$$Di = A\int_T \left(\beta\tau^\alpha t^{\beta-1} + \alpha\tau^{\alpha-1}\nabla\tau\cdot\vec{u}\right) dt$$

Table 2: Fitted values for various power-law models for blood damage.

Reference: Model Type	A	α	β
Giersiepen: Hemolysis	3.62e-5	2.416	0.785
Giersiepen: LDH	3.31e-6	3.075	0.77
Mitamura: Hemolysis	1.8e-6	1.99	0.765
Boreda et al.: PSF	1	1	0.452
Approximation: Hemolysis	1*	2	1

There are two problems with this approach. The first is that it assumes that RBCs do not disturb the flow and that they always follow the path-lines. An extensive amount of research has gone into fluid-particle flow and it is unlikely that the RBCs can be treated in this manner (70, 71). In fact, Karino and Goldsmith reported seeing platelets and RBCs migrating out of the recirculation zone of a sudden expansion. The second problem with using streamlines is that the results depend on the starting point of the particle. A large number of path-lines must be used in order to get a statistically accurate measure of blood damage. Also, particles will not enter stagnation zones without some form of stochastic modeling, or unless they a driven into it by momentum.

An improvement to this would be to solve the flow in the Lagrangian frame of reference, where the Di becomes a time varying parameter attached to each node of a FEM problem. This is often difficult to do because it requires careful handling of the mesh in order to avoid element inversion, low quality elements, and overly coarse meshes (72, 73).

Due to the current challenge in calculating the PL damage models; this thesis will adopt an Eulerian frame of reference. This could be seen as a loss of accuracy, but it is also a way of minimizing the Di over the whole fluid. Secondly, the shear stress tensor must be converted to a scalar quantity, such as $\mu\dot{\gamma}$ or maximum principal shear, as suggested previously. There are other matrix norms such as the von Mises stresses, the octahedral stresses, wall shear stress, and the Tresca criterion. But $\mu\dot{\gamma}$ and the maximum principal shear are the two most commonly used ones in fluid dynamics. Finally, the temporal component of shear history is estimated using the *residence time*, which is the time required to traverse an specific distance along the flow

pathline. It may be evaluated locally in each element using CFD, in which case it is taken as the ratio of element diameter to the particle speed. Unfortunately this method loses the directional sense, meaning reverse flow and recirculation, will give the same results as forward flow.

There are several sets of parameters that have been suggested for the PL model. Since the model of Mitamura et al. has the smallest difference between α and β it should give the best balance between shear and velocity (67). The model will be approximated using α equal to two and β equal to one as well as the values originally suggested by Wurzinger. This set of parameters was chosen for several reasons. Firstly, the fit of Mitamura et al, showed α to be almost 2 and β to be almost 0.75. Secondly, other models tend to favor shear stress to a greater extent than Mitamura. The fit of Giersiepen et al. was closer to 2.4 and 0.785 respectively for hemolysis, and 3.0 and 0.77 respectively for LDL. Using a lower value of α and the higher value of β, gives a greater balance between the two terms, where using a high value of α would allow shear stress to dominate over residence time. This study also evaluated the PSF, which uses an α equal to 1 and a β equal to 0.5.

Burgreen proposed that acceleration forces contributed to blood damage (74). Acceleration can be determined in both the Lagrangian and the Eulerian frame of reference. The Lagrangian approach involves calculating the acceleration experience by a particle, or *packet* of fluid, as it moves through the flow domain. Determining the acceleration in the Lagrangian frame has the same drawbacks as calculating the power-law blood damage models in a Lagrangian frame. It also suffers from the same drawbacks as the Lagrangian formulation of the PL blood models. The Eulerian frame has components that take into account the acceleration in terms of both time $\left(\frac{\partial \bar{u}}{\partial t}\right)$ and location $\left(\bar{u} \cdot \nabla \bar{u}\right)$, therefore the acceleration force was only measured along in the stream-wise direction.

If the acceleration changes drastically over the length of the cell, the one end of the cell will be accelerating with respect to the other points. This would result in the cell stretching and could possibly cause cell rupture. If a particle experiences vastly different acceleration across its surface, it may undergo critical deformation. It is therefore reasonable to include the gradient of acceleration to the list of objective functions. The gradient was only used in the stream-wise direction.

The final perspective we wish to investigate is extensional strain. By virtue of Umezu's studies of hemolysis in stenotic nozzles, it is known that hemolysis is strongly affected by the

nature of the flow at the entrance of a contraction (31). In Umezu's studies, the hemolysis was significantly reduced (40%) by making only slight modifications to the contraction geometry, like tapering or rounding. Such modifications did not necessarily decrease the shear stress exposure, indicating that a different field variable is more likely responsible for a significant portion of hemolysis. One of the proposed causes is extensional strain rate (a.k.a. elongation). This variable is commonly studied in the context of polymer flow where it is calculated using the diagonal components of the shear rate tensor, **D** (75).

1.2.2 Estimators of Recirculation and Stagnation

The second class of functions aims to quantify the recirculation and stagnation of the flow. **Recirculation zones** and **stagnation areas** have long been considered points of platelet adhesion and thrombus formation (76-78). Several authors have recommended using confluency, or the flow deviation angle, and stagnation area as design objectives, but there are various ways of defining confluency (63, 79). This prompted us to independently develop our own indices that are specifically appropriate for the current application. **Residence time**, **Peclet Number**, and **Damkohler Number** were also analyzed because of their relevance to convection-diffusion-reaction equations.

To compute confluency using flow deviation requires the identification of a desired flow direction (79). For a cannula, this was selected to be the unit vector normal to the local cross section. (This is not to be confused with the *desired flow field*, which is left to the preference of the designer.) Another possible method of determining preferred direction would be to reference the potential flow solution. Similarly, the Stokes flow solution would be another possible choice for the preferred direction, but this could create problems in a 3D cannula design. These methods would remove any bias from the user, and makes it possible to define flow for a wide array of shapes. Once the desired flow direction is established, the confluency can be computed from the deviation angle between the desired flow path and the simulated flow field.

Stagnation area is another common objective function that is usually not well defined (79). We will however consider stagnation as points where the flow speed drops below 5% of the mean flow. The area can be found by integrating a level-set function, which is 1 if the flow is below threshold and zero elsewhere (80).

Residence time is another factor that can be linked to thrombus deposition. A flow region that is well "washed" will have low residence times and high clearance, while recirculation zones will lead to infinite residence times and poor clearance. The residence time is a Lagrangian variable, but will be estimated in the Eulerian frame of reference as the reciprocal of fluid speed divided by characteristic length (e.g. element diameter). This approximation eliminates directional dependence from the objective function.

Two common non-dimensional numbers, **Peclet Number** and **Damkohler Number**, complete the set of objective functions studied in this research. These have not been used in the literature for the optimization of blood-wetted devices. The Peclet Number is used in convection-diffusion problems to measure the ratio of convection to diffusion. The Damkohler Number is used in chemical processes to compare the rate at which reactions are occurring with the rate at which the reactance are being removed from the area by convection, diffusion, or both. Optimization of the flow path can only change the removal of reactants, so clearance caused by diffusion is not used. These two indices naturally fit into the study of agonist-induced platelet activation, platelet aggregation, and thrombus formation because all three phenomena have been modeled as convection-diffusion based chemical reactions (4, 5, 81).

1.3   NUMERICAL METHODS FOR SOLVING PARTIAL DIFFERENTIAL EQUATIONS

Conventional testing is time consuming and requires the construction of a prototype device, which can be costly. It is possible to substitute live testing with numerical simulation in order to avoid the construction of a prototype. Numerical simulations have been developed for electromagnetics, fluid flow problems, structural analysis, convection-diffusion-reactions, heat conduction, and other physical phenomena.

1.3.1 Finite Element Method

Shape optimization involves linking a numerical optimization algorithm with a partial differential equation (PDE) solver. There are several methods for solving PDEs, but the most popular methods are the Finite Difference Method (FDM), the Finite Volume Method (FVM), and the Finite Element Method (FEM). Each method has its advantages and disadvantages, but a detailed discussion of each method is beyond the scope of this work. The FDM is the simplest to implement, but is not flexible enough for shape optimization since it does not readily conform to curved boundaries. The FVM is more flexible, but has not gained wide field acceptance because boundary condition can be difficult to implement. The FEM enjoys extensive use in most areas including fluid dynamics, solid mechanics, and electromagnetism. FEM is also proven to be efficient and accurate for solving fluid flows (82). Not only can the FEM conform to complex boundaries, but FEM can also handle various boundary conditions.

1.3.2 FEM for Fluid Flow

The solution of fluid flow equation, particularly the NS equation, has been studied in great detail (82). When solving NS-like equations including viscoelastic fluids, a mixed order Petrov-Galerkin Method should be used for stability. To do this, the elements for velocity must be at least one order higher than those for the pressure. If not, the method will not satisfy the Ladyzhenskaya-Babuska-Brezzi (LBB) condition for stability. The standard Galerkin method must be further stabilized, hence Petrov-Galerkin, in order to eliminate oscillation in areas where the flow changes rapidly. This can be done using artificial viscosity as is done in the FDM. The problem with this technique is that the actual equation is altered (82). Accuracy is traded for stability. Stream-wise Diffusion Method (SWD) is better because it only increases the viscosity along the streamline and not over the whole field. This does not smear the information across the stream-lines where the gradients are usually highest as the AVM does (83, 84). Unfortunately solution still may not be consistent with the original PDE, although it is more accurate than the artificial viscosity method.

The concept of the SWD led to the Galerkin-Least-Squared Method (GLSM), which is more precise (85, 86), and derived so that the FEM solution is consistent with the PDE. The

13

GLSM also includes variational terms relating to the pressure so the LBB condition is satisfied automatically and equal order elements can be used to approximate the PDE. The drawback of the GLSM is that it requires several adjustable parameters that are element-dependent and whose physical meaning has not been determined.

Other methods try to decouple the pressure and velocity terms on order to satisfy the LBB condition. The most popular approach is the Penalty Method (PM), which relaxes the incompressibility condition, and replaces pressure with a penalty function of the divergence of the velocity (82, 87). This method reduces number of unknowns down to just the velocity terms. The PM does have several drawbacks. The first is that there is no accurate method for determining the penalty function. This method does not calculate the pressure to the same accuracy as the other methods. Finally, the coefficient matrix is nonsymmetrical and ill-conditioned, which could lead to yet more errors and/or failure to converge to a solution (88, 89).

1.4   SHAPE OPTIMIZATION

Analyzing and entire design space in a systematic fashion would be difficult and time consuming and costly to do with conventional prototyping or simulation. Design time can be reduced by coupling numerical simulation to numerical optimization routines. This also allows for an efficient search of the design space in order to find the best possible solution, assuming that the goal or best design qualities is easily defined.

1.4.1   General Topics in Optimization

Optimization refers to a collection of methods for finding a set of parameters of a system that in some way can be defined as *optimal*. Usually the parameters are determined by minimizing or maximizing a function, called the **objective function**, which is some mathematical way of measuring a goal, a value system, or desired design quality. One of the simplest examples of an optimization technique is the least-square fitting. The objective function is the root mean square

of the difference between the data and the function being fitted, and the optimal parameters lead to the best approximation. The standard form of an optimization problem is:

$$\text{minimize} \quad F(\vec{x})$$
$$\vec{x} \in R^n$$
$$\text{subject to}$$
$$Gi(x) = 0, \quad i = 1,...,m_e$$
$$Gi(x) \leq 0, \quad i = m_e + 1,...,m$$
$$x_l \leq \vec{x} \leq x_u$$

Most of the information presented in this section can be found in a standard text book on optimization (90, 91), but specific references are places where they are needed or where they can help clarify a technique.

Obtaining a solution efficiently and accurately depends on several factors, such as the number of constraints, the number of design parameters, as well as the behavior of the objective function and constraints. Finding the optima of linear and quadratic problem is uses well-established methods. For non-linear or higher order problems (NLP) iterative techniques must be implemented to find the optimum. Optimization routines are also broken down into unconstrained and constrained optimization. Most techniques have been developed to deal with unconstrained problems, so various methods are used to combine the constraints and the objective function into a new objective function.

Several steps generally describe the standard optimization algorithms for the NLP. These steps are determining a search direction, a line search, and evaluating the optimality of the new point. These steps are repeated until the minimum or maximum are found. Most of the methods for determining the search direction and doing the line search are LP or QP problems. The following sections will discuss some of the most common algorithms for doing these sub-problems, as well as the commonly used overall methods for optimization.

Converging to a *global* optimal point is difficult. Most routines will only find the global minimum if the objective function and constraints are concave throughout the entire domain, or if the initial conditions are specified close enough to the global minimum. Therefore, it is common repeat the optimization several starting points. This usually allows the solver to find a global optimum, although there are no guarantees that this is the case.

The final topics that will be discussed are common methodologies for dealing with constraints, multi-objective optimization, and the formulation of the optimization for PDE

constrained problems. For the interest of space, optimization topics that are not relevant to the current project will be omitted here, including genetic algorithms and discrete point optimization methods. The ensuing optimization methods will be discussed in terms of a minimization problem, which tends to be standard procedure. Maximization routines can apply the same techniques with slight modifications, but a maximum can be determined by minimizing the negative of the objective function\

1.4.1.1 Determining the Search Direction

The first step in most optimization routines is to determine a search direction. These algorithms use gradient information to determine the general direction toward the minimum. The simplest gradient-based method that is commonly used to find the search direction is called the *steepest decent*. The search direction, p, is the negative of the gradient, since the gradient points in the direction of maximum increase. This algorithm is guaranteed to converge and does so linearly. However, in the case that an objective function is elongated in a particular parameter direction the convergence is slow, and can take a large number of iterations to converge.

A more sophisticated method for determining the search direction is based on Newton's Method for root finding. The optimal point of a function f is defined as where the gradient is zero, and so Newton's equation, given by

$$-\nabla f = H\, \vec{p},$$

where H is the Hessian matrix, and p is the search direction. This method has the advantage that it shows quadratic convergence around the optimal point yet does not suffer the problems associated with steepest descent. But, unlike the steepest descent method, the Newton's method is not guaranteed to converge. This method will find a search direction toward the nearest optima, whether it is a minimum, a maximum, or a saddle point. If the Hessian matrix, H, is positive definite, then the routine will head in the direction of a local minima. Positive definiteness implies that:

$$x^T A x > 0 \quad \forall x \in R^n \neq 0.$$

Several techniques have been developed in order to deal with situations where the Hessian is not positive definite. The simples method is to use the steepest descent until the Hessian becomes positive definite. This method gives rapid convergence near the optimum, but has all of the drawbacks of the steepest descent method. The second method is called the Picard

Method, where the Hessian is only approximated. Components of the Hessian that could lead to it becoming negative or indefinite are dropped. This method does not show the quadratic convergence as Newton's Method, but it does not suffer the drawbacks of the steepest descent method. However, Picard's method requires that the Hessian be calculated mathematically which is not always possible. Other methods for approximating the Hessian in a manner that keeps it positive definite can also be used. These will be discussed a little later in more detail.

The preceding discussion has not mentioned how the gradients and Hessian are obtained. Ideally, the best results occur if the gradients can be calculated directly through differentiation or variational calculus, but most practical problems do not lend themselves readily to differentiation. In this case the derivative can be calculated using finite differences, which involves perturbing each optimization parameter slightly. This can be difficult because the truncation error can adversely affect the optimizer. In some cases the numerical noise can set up local minima or numerical oscillations, which cause difficulties in convergence. Also, numerically calculating the derivative can be computationally expensive for large problems such as those using CFD or other PDEs.

The Hessian matrix would require additional function evaluations in order to use finite differences to determine its values (92). The problem with numerical differentiation is that it quickly becomes noisy and so higher derivatives become less and less accurate. Even if the Hessian is reasonably approximated using finite differences, there is no guarantee that the matrix will be positive definite. Therefore the Hessian is usually approximated using more sophisticated the methods described by Broyden (93), Fletcher (94), Goldfarb (95), and Shanno (96) called BFGS. This method uses the values of the function, as well as the derivative information (either exact or approximated), to build up the curvature information. The Hessian is initially set to a positive definite matrix, such as the identity matrix, and is updated at each iteration using the equation:

$$H_{k+1} = H_k + \frac{q_k q_k^T}{q_k^T s_k} - \frac{H_k^T s_k^T s_k H_k}{s_k^T H_k s_k},$$

where

$$s_k = x_{k+1} - x_k = \alpha \, \bar{p}$$

$$q_k = \nabla f_{k+1} - \nabla f_k$$

This method guarantees that the Hessian will remain positive definite. It is also possible to update the inverse of the Hessian using a similar method so that the search direction can be found without a matrix inversion (97, 98).

The Newton-based methods usually involve finding the search direction using an iterative method. It is often the case, that only a few iterations are used to determine p, to reduce computational time.

1.4.1.2 The Line Search

A line search takes place once an appropriate search path is found in order to determine how far to move along the search direction. It is another minimization sub-problem, except that the function is only minimized along a single direction in the form:

$$F(\vec{x} + \alpha \, \vec{p})$$

where α is a constant chosen to strike a balance between convergence and stability.

Several methods are used that reduce the time spent in this subroutine; just as the search direction was modified to save time. The first method is an interval halving method, where α is set to 1 for the initial step. The function is evaluated and checked to see if it decreased a sufficient amount. If the function does not decrease sufficiently, the step size is halved until the required reduction occurs. If the step-size becomes too small, the routine fails. This commonly occurs if the angle between the search direction and the contour line is small. More advanced methods use quadratic approximations, cubic approximations, or a mixture of both to find a minimum faster. The minima of these functions can be found analytically, and allow for α to be extrapolated beyond 1. Normally, extrapolation is numerically undesirable, but if the extrapolated point does not reduce the function, it increases the range over which alpha can be interpolated.

1.4.1.3 Evaluating Optimality

The *optimality condition* is ultimately defined where the gradient of the objective function is zero or at the lowest value along in the domain. In practice, an optimality condition may be defined by the gradient below a small threshold value. This is a relatively straightforward calculation. First, the gradient of the new point is calculated, which will also be used in the next Newton step if the point is not optimal. The second step is to evaluate the norm of the gradient,

which should be zero at the optimum. For a constrained problem, the minimum might be outside of the allowable parameter range. In this instance the point along the boundary with the lowest value is the minimum.

1.4.1.4 Handling Constraints in Optimization Problems

The routines for finding optimal values are developed for unconstrained problems, but most problems are constrained in some fashion. A problem is constrained if there are restrictions on the values that the optimization parameters can assume. Most engineering problems are constrained by logic, user requirements, physical principles or limits, or other practical issues. Constraints can take on various forms such as bounds on certain parameters or nonlinear and linear relationships – often represented by auxiliary equations. Equality constraints actually reduce the size of the problem, since one parameter can always be expressed in terms of the others. Constraints also help improve the convergence qualities of the optimization routines.

In constrained optimization, the problem must be transformed into a new unconstrained formulation using various methods. Early methods involved developing penalty functions that would increase rapidly as the parameters came close to violating the constraints. More modern methods have been developed using Lagrange multipliers, since these early methods were inefficient, difficult to implement, and altered the design space. The problem would now be considered unconstrained, but with steep penalties for violating the constraints, hence driving the solution back into the *feasible* region.

1.4.2   The Sequential Quadratic Programming Method for Optimization

The favored gradient-based method for unconstrained optimization is the Quasi-Newton method. This method builds up the curvature information at each step, and uses it to approximate the objective as:

$$x^T H x + \nabla f^T x + c = F(\bar{x}) .$$

The method typically uses the BFGS to update the Hessian, but other methods can also be used. The line search is done using a mixed quadratic and cubic line search method.

SQP is the most efficient, accurate, and successful version of constrained optimization routines (99). This method closely follows the Newton's method for constrained problems (100-102). The SQP method rewrites the constrained problem into the form:

$$L(\vec{x}, \lambda) = F(\vec{x}) + \sum_{i=1}^{m} \lambda_i G_i(\vec{x})$$

where

$$\lambda \begin{cases} = 0 & \text{Constraint not violated} \\ > 0 & \text{Constraint Violated} \end{cases}$$

using the Lagrange multiplier method. The Hessian for L is updated using the quasi-Newton approach.

1.4.3 Multi-Objective Optimization

Although single objective optimization can produce good working models, it is often impractical. Real-life design problems almost always involve multiple and competing goals, such as the present study wherein several indices are used to evaluate blood damage. Usually the objective function is represented by a vector of objectives, but the problem with this formulation is that the tradeoff between each objective function is not known a priori. In fact, no unique solution can be found for MOO; only a range of solutions can be determined, depending on the weighting applied to each function.

The MOO problem can be stated in the same fashion as the unconstrained problem, except now the objective function is a vector. When there is not a unique solution to the MOO the objective function should be analyzed using Pareto optimality (103, 104). Here the MOF refers to the combination of all objective function, while OF will refer to each individual function. Strong Pareto optimality occurs when at least one OF is at a minimum when the MOF is at a minimum. Weak Pareto optimization is where the MOF is at a minimum, but none of the OFs are actually at a minimum (105). Pareto optimality is characterized by the concept of noninferiority. A noninferior solution is where improvements to one OF requires a degradation of another function (103, 104).

The first step in MOO is to transform the OF through normalization. This prevents any single function from dominating the others based only on its magnitude. The simplest

transformation, which will be referred to as KS transformation in this thesis, was presented by Koski and Silvenoinen (106):

$$F_i^{norm} = \frac{F_i}{F_{min}} \, ,$$

which normalizes the OFs so that their value reaches unity at their optimal points. Koski previously presented a second method (106, 107):

$$F_i^{norm} = \frac{F_i - F_i^{min}}{F_i^{max} - F_i^{min}} \, ,$$

which normalizes for both magnitude and variation. This transformation, referred to in this thesis as the Koski transformation, is normalized from 0 to 1. These second step is to determine the relationship between the OFs. The MOF can formed using numerous techniques, but the most basic is the weighted sum method (105):

$$MOF = \sum_N w_i F_i^{norm} \, .$$

There are many methods for the selection of the weights in order to avoid arbitrary selection (105). Most of these methods involve ranking the OFs in order of their importance, but for this thesis each form of blood damage will be given a weight of 1, meaning none has a higher priority than the next. After the MOF is determined, the problem is ready for any standard optimization routine.

1.4.4   Shape Optimization in Fluid Dynamics

Shape optimization of a PDE problem has a similar structure to a standard optimization problem. The general form the problem is given by:

$$\min F(\bar{u}, \bar{\pi})$$
$$w/r \; \bar{\pi}$$
Constrained by :
$$C(\bar{u}, \bar{\pi}) = 0$$
$$G_i(\bar{\pi}) = 0 \quad i = 1,..., m_e$$
$$Gi(\bar{\pi}) \le 0 \quad i = m_e ,..., M$$

Here the weak form of the PDE is treated as an additional constraint on the problem, and $\bar{u}$ refers to the solution of that PDE. The PDE is solved for a given set of shape parameters and the

solution is used to calculate the OF. Since a PDE is a spatial problem, the OF will be calculated as the norm of the function relating to blood damage. Three norms will be considered for this study and are defined as:

$$\left\| f(\bar{x}) \right\|_i = \int_\Omega f(\bar{x}) d\Omega : \quad \text{Integration Norm}$$

$$\left\| f(\bar{x}) \right\|_\infty = \max(f(\bar{x})) \, in \, \Omega : \quad \text{Infinity Norm}$$

$$\left\| f(\bar{x}) \right\|_a = \frac{\int_\Omega f(\bar{x}) d\Omega}{\int_\Omega d\Omega} : \quad \text{Average Norm.}$$

Derivatives for the PDE constrained problem are not well defined. Most algorithms rely on finite difference approximations of gradients, and use an approximate Hessian using BFGS or the like. Two other methods are for determining the gradients are sensitivity analysis. Sensitivity analysis use calculus of variations for determine the sensitivity of the OF to a design variable, which includes a sensitivity of the flow variables to the design variable. The sensitivity analysis of the weak form of the PDE is used to find the sensitivity of the flow variables. This method is faster that a finite difference method because the sensitivity equations are linear, where the NS equations are non-linear. Unfortunately this technique requires some method of determining the sensitivity of the PDE to the shape parameter, which may be difficult to define.

2.0   METHODS

This study focused on the optimization of a two-dimensional fluid dynamic domain representative of a blood conduit, or cannula. The domain was comprised of a 90 degree arc (or "elbow") with prescribed boundary conditions, including a flow rate requirement of 6 liters per minute.

2.1   NUMERICAL METHODS

2.1.1   Computational Fluid Dynamics Using FEMLAB

All simulations in this study were performed using FEMLAB (COMSOL, Inc.), a multiphysics finite element analysis package. The simulations were run with Taylor-Hood finite elements: quadratic in velocity and linear in pressure. The mesh elements were triangular in 2-D and tetrahedral for 3D. The mesh was refined until it was fairly dense, approximately 4,000-5,000 elements. A continuation method for flow rates starting at zero and increasing up to 6 L/min was used to ensure stable conversion. The non-linear tolerance was of the order –4 for the early continuation steps, but was increases to –7 for the final step. This helped to reduce the computational time, without decreasing the accuracy of the scheme.

The inlet boundary condition was prescribed by an uniform velocity profile, indicative of the entrance flow from the heart. The outlet condition was set to zero traction (pressure of 0 dynes/cm^2) and with a tangent constrained normal to the exit plane. The blood was treated as a Newtonian fluid with a viscosity of 3.5 cP and a density of 1.05 g/cm^2. This is the commonly used asymptotic value for blood at room temperature. It has been shown that simulations using a Newtonian approximation can be quite accurate when the Reynold's number is sufficiently large

and the blood viscosity is taken at an average shear rate for the flow (74). The viscoelastic properties of blood were ignored because they usually occur at very low shear rate (<2/s) and the shear rate of this study was several orders higher (> 200/s).

2.1.2   Optimization Using the SQP Method

The optimization was performed in several steps. The first step was to minimize and maximize each of the individual objective functions for the 2-D cannula. Two multi-objective optimization methods were then evaluated in order to determine the best method to combine the objective functions. The optimization was done using the SQP method, which is built into the optimization toolbox of MATLAB (by Mathworks). When needed, the maximum was found by minimizing the negative of the objective function, since the SQP method only solves for minimums. The optimization routine was started at several different points in order to find the global minimum. These starting points included the minimum and maximum values from the design space analysis in 2-D. The convergence rate, optimum values, and shapes were analyzed for design characteristics.

2.2   ANALYZING OBJECTIVE FUNCTIONS

2.2.1   Qualitative Analysis of Objective Functions

Prior to performing the actual shape optimization, a rigorous evaluation and comparison of the objective functions was performed by simulating flow in two-dimensional channels that have been selected for particular flow behavior. Although it is possible to get a numerical comparison of each shape, the primary focus will be to observe behavior of the blood damage functions in each flow field. Both good quality (low shear and no recirculation) and bad quality designs were selected (Figure 1). The first good cannula was designed using the upper right quadrant of a ring,

24

while the second came from the preliminary results of the 2-D optimization for the Peclet Number.
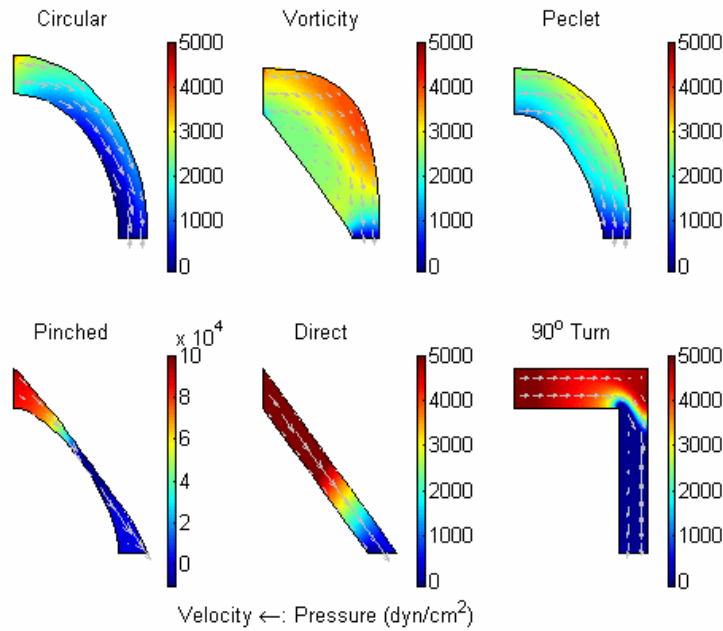
Figure 1: Flow through selected cannula plotted with pressure contours and velocity vectors.

Several other designs were chosen because of the poor flow features that they generate, such as zones of high stress and recirculation. The most obvious of the bad designs, was a cannula that has been "pinched off" at its center, thereby throttling the flow. Figure 2 shows the recirculation zones in the bad cannula designs. The flow of blood in a stenosis has been studied extensively (108-111), and it is known to cause a high rate hemolysis at the throat and thrombus formation downstream of the contraction where a recirculation region forms. A pinched cannula behaves in a similar manner as a stenosis. The 90° cannula develops two recirculation regions. The first is in the upper right corner and the second one is located on the inner wall just distal to the turn. These two recirculation zones act to constrict the flow through this section and cause a jet similar like the stenosis, but weaker. Another poor feature of the square cannula is that there is a zone of high stress that forms just before the turn on the lower wall.
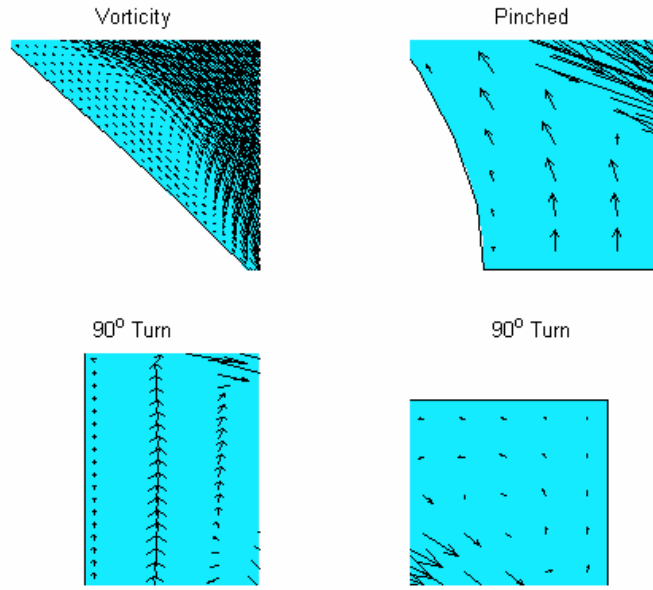
Figure 2: Recirculation regions of bad cannula designs

The two more bad designs were analyzed in this part of the study. The third bad cannula design is based on the preliminary optimization results for vorticity. In order to reduce the vorticity, the walls expand to reduce velocity, which produces a large recirculation zone along the inner wall. The final bad design is not physically accurate, but is a purely mathematical model that provides useful intuition into the objective functions. The inlet and outlet are placed in position for the inflow cannula of the Streamliner VAD, and the walls were composed of straight lines. The flow is forced to turn quickly upon entering and exiting the cannula, which results in high shear stresses along the walls.

The flow field was calculated for each cannula using CFD. The velocity vector field and the pressure field of each flow were plotted in order to verify the flow each channel. Once this was done, the objective functions were analyzed in several ways. The damage functions were plotted over the entire domain and visually compared to see how they identified important flow features. Secondly the objective functions were analyzed using all three norms and the results were tabulated and compared by ranking the designs.

2.2.2   Quantitative Analysis of Objective Functions

Although the qualitative analysis of objective function is insightful, it is more desirable to do a more rigorous mathematical comparison of the objective functions. This was done in several steps. The first step was to analyze the design space that was selected for the optimization of the 2-D cannula. The correlation between various objective functions can then be made using the resulting data set. It is possible to determine whether objective functions are independent, by studying the correlation matrix. The second step was to use principal component analysis to determine the number of objective functions that are necessary to reasonable describe all modes of blood damage. Statistical analysis was used to mathematically analyze the behavior of the objective functions, in order to determine the variance over the design space and to estimate robustness of the function. Calculus of variations was used to determine the convergence characteristics of some of the objective functions in order to determine if they would be suitable to use in standard optimization routines.

In order to compare the objective functions in a more mathematical way, we examined the design space for the 2-D cannula. The design-space is composed of all possible conformations that the shape can assume. In this analysis we discretized the design space into select points spanning the allowable ranges. Figure 3 shows the 2-D cannula and its design space. The design has a fixed inlet and outlet at the approximate location for the placement of the Streamliner cannula. 3rd degree Bezier-Curves are used to describe the side walls of the cannula. The end points of the Bezier curves are fixed at the inlet and outlet, and the interior-Bezier points are constrained to ensure the tangency of the cannula walls at its attachment points. Each point was given an upper and lower bound to keep the points from overlapping, which would cause a singularity in the shape. An additional inequality constraint was applied to prevent the upper and lower curves from overlapping. This geometry allows for a flexible design, yet maintains a realistic boundary for the cannula.

27
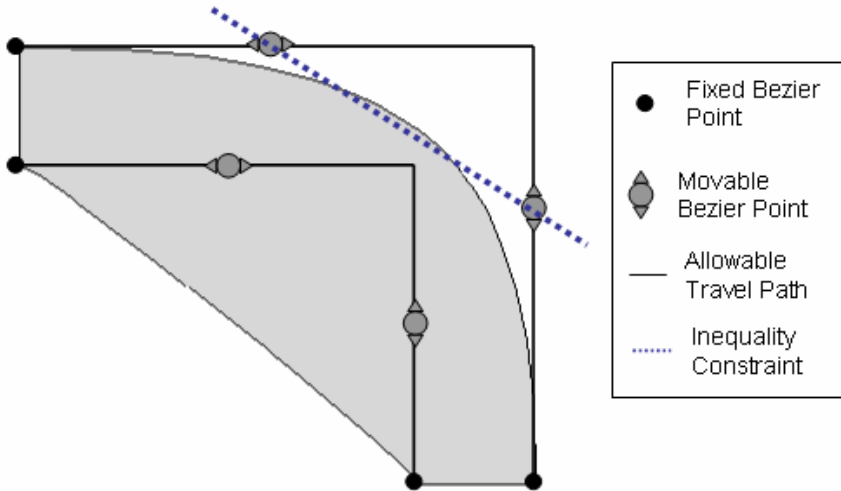
Figure 3: Design space for the 2-D cannula.

The design space was discretized by dividing the range for each parameter into six points and removing any point combination that violates the inequality constraint. The flow was solved for each set of discrete points. MATLAB was then used to determine the correlation between each objective function and to do the principal component analysis (PCA). The eigenvalues of PCA can help determine how many function provide distinct information to a system. If two functions are highly correlated, then one function can be used to represent the other so one function can be dropped. MATLAB was also used to calculate the statistics: mean, median, maximum, minimum, and the variation; and to plot the histogram for each objective. The histograms will tend to be skewed left or right if there is a large difference between the mean and the median. The skew is indicative of the curvature of the objective function around the optimal value. For example if the distribution is skewed toward the optimal value; that point is relatively flat and robust. If the distribution is skewed away from the optimal point; that point is sharply curved and very sensitive to small design changes.

2.3   OPTIMIZATION OF A 2-D CANNULA

While it is the ultimate objective to optimize the design of a blood cannula in three-dimensions, this study adopted a two-dimensional simplification for several reasons. The most obvious

motivation is because of dramatically reduced computational time thereby allowing more simulations to be performed in a practical span of several months. The additional speed also enables insight to the sensitivities and behaviors of the objective functions upon the optimum shape. The methods that were developed and refined in this two-dimensional analysis can be readily expanded to 3D.

The characterization of the geometry is crucial for determining the best design. Although the method for describing the 2-D geometry described in the previous section only has four degrees of freedom, this should be sufficient for this problem. The SQP method (described in 4.3.3) was used to perform both the single-objective optimization and the multi-objective optimization. Each objective function was individually optimized in order to analyze its effect on the geometry, but also so that these values could be used in the multi-objective optimization problem. The Koski approach was applied to the multi-objective optimization because it normalized both the magnitude and variation of the function, which gives each objective function equal footing.

The optimal designs were analyzed visually by observing the general trend in the shape. The flow within the cannula was also checked for flow features, but also by examining the other objective functions. The multi-objective design was also analyzed in order to find out the percent difference between the optimal design and the MOO design. This is an estimate of how much performance is "lost" from each objective in order to accomplish the multi-objective optimization.

3.0 RESULTS OF OBJECTIVE FUNCTION ANALYSIS

It is important to understand the behavior of each function as it pertains to quality and low quality designs. It is also important to have and indication of the ability of each function to indicate flow regions that would cause increased blood damage. The following experiments determine which functions provide the best information for use in a multi-objective optimization problem.

3.1 QUALITATIVE ANALYSIS OF OBJECTIVE FUNCTIONS

The CFD solutions for the flow fields provide good insight into the flow through each cannula. Figure 1 shows the flow features for each cannula. The CFD results confirm that there are recirculation regions in the 90° turn, the minimum-vorticity cannula, and the pinched cannula. The elevated shear stress can be seen in the straight cannula, the 90° turn, and the pinched cannula. The jet regions are also apparent in the pinched cannula and the 90° turn. There are also high stress regions at the inlets, which are a result of the rapid deceleration of the flow at the inlet. This indicates that a better boundary condition would be advisable, but the inlet flow for a cannula is typically blunted and not fully developed.

The features found when plotting the objective functions describing hemolysis and shear induced platelet activation had similar features. The actual magnitude of the plots varied, but the similarities were distinctive. Figure 4 shows six of these functions, plotted in the 90° cannula. Some of the features that are prominent are the contracted regions showing the boundary layer formation and the boundaries of the recirculation regions.

Colorbars use a $\log_{10}$ scale
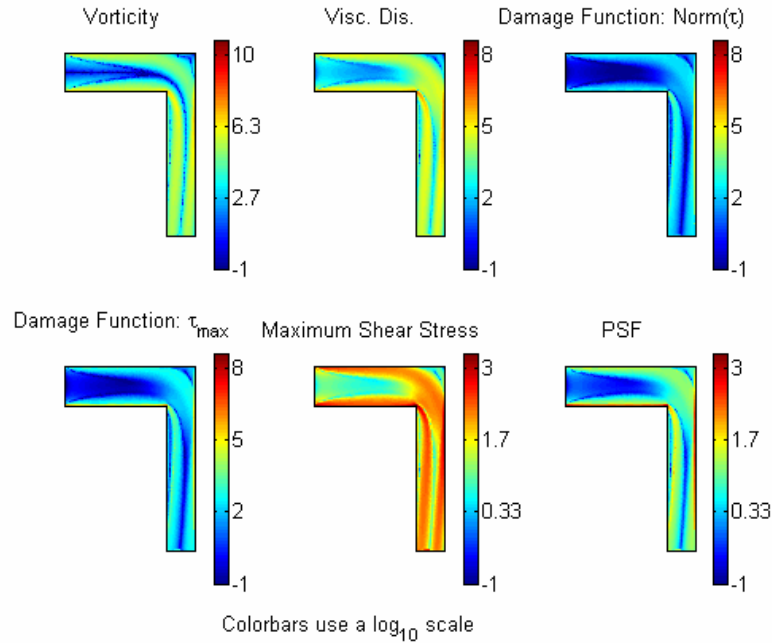
Figure 4: Field plot of the several functions that represent shear induced hemolysis.

Most of the functions relating to recirculation and stagnation failed to catch all of these features, particularly those just distal to the contraction in the pinched cannula and the inner wall of the square cannula. (See Figure 5) The flow angle clearly shows the presence of all of the recirculation zones. Peclet number, residence time, and stagnation area all fail to identify these recirculation zones because the speed of the recirculation is high in these two regions. The residence time is slightly larger in the recirculation zone (100.75), but is not very distinct when compared to the boundary layer (104). Stagnation area only shows the regions where there is a boundary between forward and backwards flow. At best, these functions show the boundary between forward and backwards flow, but they do not show the entire area as well as the deviation angle. The vorticity function can pick up these high-speed zones, but fails to pick up slow recirculation cells, like the one that forms in the minimum-vorticity cannula.
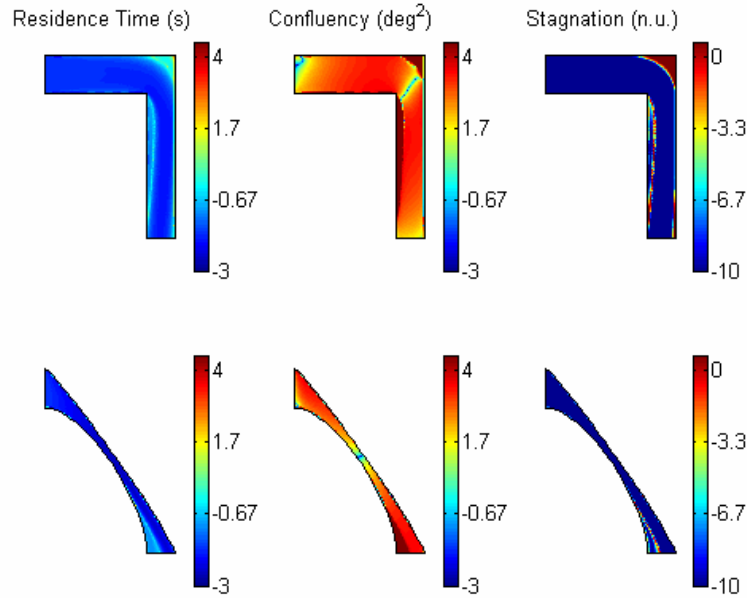
Figure 5: Plot of function that relate to stagnation. The color is plotted logarithmically.

The effect of area on the objective function is another important issue that is raised by the qualitative analysis. The maximum-Peclet Number cannula had a lower optimal value (cm^2) for the Peclet objective function than the squared cannula. There are two reasons for this. The first is that the geometric flexibility of the design does not allow for the cannula to take on that particular shape. The second is that for a given flow rate, the longer cannula flow path, the higher integral norm. In this case, the average norm is a better selection.

Table 3 shows the values of each objective function using the integration norm. The yellow highlights indicate the best value in each category, while the red type indicates the worst value. The best overall design is the maximum-Peclet Number cannula. It had the lowest viscous dissipation, PL damage model, stagnation, and PSF values. The circular cannula had similar values to the minimum-vorticity cannula. The worst design was clearly the pinched cannula, which does show that most of the objective functions would prevent this type of design. Stagnation area and flow deviation angle both found the large recirculation zone in the minimum-vorticity cannula, and consequently hurt its ranking. The infinity norm does not provide much in terms of useful information, particularly since most of the functions do not physically justify this norm. The minimum Peclet number is always zero at the wall, while

32

maximum stagnation is always one when flow is below threshold. The infinity norm can be used for the shear dependent objective functions.

Table 3: The evaluation of each objective function in the selected designs.

Cannula Selections

Objective Function	Good Cannula	Direct Cannula	Squared Cannula	Minimum Vorticity	Pinched Cannula	Maximum Peclet #
Vorticity	4.16E+05	1.59E+06	8.66E+05	2.78E+05	1.68E+07	9.39E+05
Viscous Dissipation	9.61E+04	1.44E+06	1.54E+05	5.59E+04	4.96E+06	1.91E+04
Damage Function 1	6.43E+07	1.60E+09	5.88E+07	2.57E+07	2.35E+09	1.02E+06
Damage Function 2	1.28E+08	3.19E+09	1.17E+08	5.12E+07	4.71E+09	2.04E+06
Damage Function 3	1.22E+7	2.93E+08	1.11E+07	4.84E+06	4.35E+08	1.96E+05
Residence Time	3.32E+03	1.40E+03	2.35E+03	2.74E+03	1.19E+03	1.25E+03
Acceleracton	5.41E+06	6.83E+08	2.36E+07	2.27E+07	1.18E+10	2.48E+07
Gradient of Acceleration	1.84E+17	2.04E+25	3.13E+18	1.46E+20	6.42E+26	3.51E+20
Stagnation Area	3.34E-01	1.41E-01	7.60E-01	1.01E+00	1.33E-01	1.25E-01
Flow Direction	1.93E+01	4.42E+03	2.98E+04	3.63E+04	1.20E+04	1.55E+02
Maximum Shear Stress	5.99E+05	2.86E+06	9.62E+05	3.46E+05	3.10E+07	1.17E+06
Elongation	9.15E+04	6.35E+05	4.78E+04	3.43E+04	7.08E+06	1.15E+05
Peclet Number	4.55E+11	4.17E+11	5.78E+11	4.80E+11	4.43E+11	4.76E+11
Damkohler Number	8.26E+00	8.14E-02	6.30E+00	8.71E+00	5.65E-02	4.43E+00
PSF	4.39E+03	1.06E+04	2.76E+03	1.72E+03	1.31E+04	2.83E+02

3.2   QUALITATIVE ANALYSIS OF THE DESIGN SPACE

3.2.1 Evaluation of the Design Space

Table 4 shows the correlation matrix for the design space using the integral norm approach. Numbers in blue type indicate high correlation values, red type indicates moderately anti-correlated values, and yellow highlights indicate the diagonal of the matrix. 1249 solutions were required to cover the entire space. The functions that have been linked to hemolysis did show

high correlation with each other (C>0.95). The platelet stimulation function also showed a reasonable correlation to the other power-law damage models (C>0.8). This was surprising since the PSF is approximately the square root of the hemolysis model. The correlation between the damage function using the maximum principal shear stress and the index based on viscous shear stress indicated that they were virtually equivalent. The acceleration force was found to correlate to the hemolysis models, but not as well as amongst each other (0.93>C>0.92 to >0.99). There were no anti-correlated functions (C<-0.75). This means that there are no one-to-one trade offs in the objective functions, so is possible to improve all of the objective functions to some extent. Peclet Number, stagnation area, confluence, and the Damkohler Number all appear to be independent of the each other and the other functions. The gradient of acceleration, although capable of determining jet flow, does not correlate with the various hemolysis models. This means that it is unlikely that this function actually contributes significantly to hemolysis.

Table 4: Correlation table for the design space analysis.

	Ref. frame	Vorticity	Viscous Dissipation	Damage Function 1	Damage Function 2	**Damage Function 3**	Res. Time
Vorticity	Both	1.0000	0.9996	0.9981	0.9981	0.9981	-0.3948
Viscous Dissipation	Both	0.9996	1.0000	0.9979	0.9979	0.9977	-0.3924
Damage F1	Lag	0.9981	0.9979	1.0000	1.0000	1.0000	-0.3759
Damage F2	Lag	0.9981	0.9979	1.0000	1.0000	1.0000	-0.3759
Damage F3	Lag	0.9981	0.9977	1.0000	1.0000	1.0000	-0.3770
Residence Time	Lag	-0.3948	-0.3924	-0.3759	-0.3759	-0.3770	1.0000
Acceleraction	Both	0.9278	0.9359	0.9259	0.9258	0.9238	-0.3193
Gradient of Accel	Both	0.7298	0.7455	0.7259	0.7255	0.7220	-0.1879
Stagnation Area	Eul	-0.1076	-0.1049	-0.0984	-0.0984	-0.0993	-0.0597
Confluency	Both	0.4360	0.4330	0.4472	0.4472	0.4478	-0.2814
Principal Shear Stress	Both	0.9996	1.0000	0.9979	0.9979	0.9978	-0.3925
Elongation	Both	0.9982	0.9995	0.9968	0.9968	0.9964	-0.3893
Peclet Number	Both	0.0926	0.0879	0.1120	0.1120	0.1117	0.3702
Damkohler Number	Both	-0.2024	-0.1951	-0.1781	-0.1782	-0.1803	-0.1194
Platelet Stim. Funct.	Both	0.8178	0.8040	0.8063	0.8065	0.8099	-0.3408

34

Table 4 (continued from left side)

Accel- eration	Gradient of Accel- eration	*Stagnation Area*	**Conflu- ency**	Principal Shear Stress	Elong- ation	**Peclet Number**	Damkohler Number	PSF
0.9278	0.7298	-0.1076	0.4360	0.9996	0.9982	0.0926	-0.2024	0.8178
0.9359	0.7455	-0.1049	0.4330	1.0000	0.9995	0.0879	-0.1951	0.8040
0.9259	0.7259	-0.0984	0.4472	0.9979	0.9968	0.1120	-0.1781	0.8063
0.9258	0.7255	-0.0984	0.4472	0.9979	0.9968	0.1120	-0.1782	0.8065
0.9238	0.7220	-0.0993	0.4478	0.9978	0.9964	0.1117	-0.1803	0.8099
-0.3193	-0.1879	-0.0597	-0.2814	-0.3925	-0.3893	0.3702	-0.1194	-0.3408
1.0000	0.9030	-0.0562	0.3678	0.9353	0.9434	0.0650	-0.0867	0.5889
0.9030	1.0000	-0.0308	0.2222	0.7441	0.7605	0.0848	-0.0338	0.3286
-0.0562	-0.0308	1.0000	0.6913	-0.1051	-0.1020	-0.0476	0.6907	-0.2559
0.3678	0.2222	0.6913	1.0000	0.4331	0.4293	-0.0352	0.3848	0.3145
0.9353	0.7441	-0.1051	0.4331	1.0000	0.9995	0.0883	-0.1956	0.8047
0.9434	0.7605	-0.1020	0.4293	0.9995	1.0000	0.0829	-0.1873	0.7883
0.0650	0.0848	-0.0476	-0.0352	0.0883	0.0829	1.0000	0.0030	0.0643
-0.0867	-0.0338	0.6907	0.3848	-0.1956	-0.1873	0.0030	1.0000	-0.4925
0.5889	0.3286	-0.2559	0.3145	0.8047	0.7883	0.0643	-0.4925	1.0000

The principal component analysis yielded eigenvalues that were ranked from the lowest to highest as shown in Figure 6. The bottom half of the figure shows the individual percent in blue, and the cumulative percent in red. The cumulative percentages indicate that only three to four of the objective functions represent more than 90% of the overall information represented by the correlation matrix. It is statistically acceptable to use only four out of 15 for the optimization method. Although four functions should be used to reach 90% of the information, three should be sufficient, since the gradient of acceleration does not appear to correlate with hemolysis.
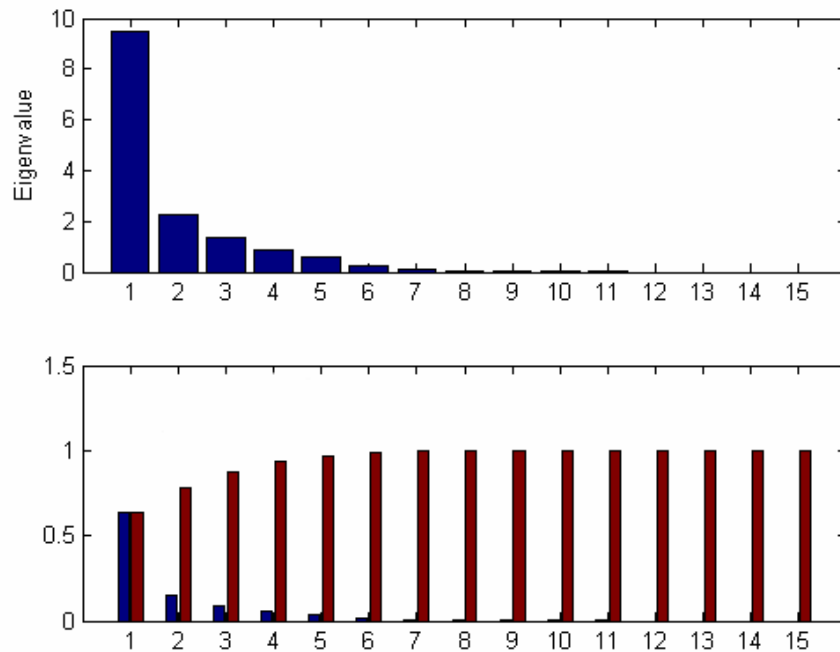
Figure 6: Plot of the eigenvalues and their information percent.

The correlation matrix for the infinity norm and the average norm were also evaluated. There were no strong correlations among the objective functions evaluated by the infinity norm, except for the PL models. They also showed little correlation to the equivalent function evaluated with the integral norm. This is most likely because these are evaluated at a single point in the flow field, where the integral and average norms are evaluated over the entire flow field. Integrals tend to smooth out noisy data. The correlation matrix for the average norm showed similarities to that of the integral norm. This is because the ratio between each function does not change with the norm.

More statistical information can be gathered from the design space study. Table 5 shows the minimum and maximum of the integral norm, the mean and medium of integral norm, and the variance of the design space. Almost all of the functions had a variance of 4-6% and several orders of magnitude difference between their max and min values. The only objective functions that had a lower variance were residence time (0.13%), stagnation area (1.37%), Peclet Number (0.06%), Damkohler Number (2.22%), and the PSF (1.43%). The acceleration force and the gradient of acceleration both had high variances, 17.03% and 65.9% respectively.

Table 5: Statistical evaluation of the objective functions.

	Min	Mean	Median	Max	Varience	Histogram
Vorticity	7.03E+05	2.23E+06	1.35E+06	7.50E+07	4.81%	Skew Left
Viscous Dissipation	2.41E+05	9.41E+05	5.34E+05	3.66E+07	5.48%	Skew Left
Damage F1	1.38E+08	6.98E+08	3.48E+08	3.14E+10	6.54%	Skew Left
Damage F2	2.76E+08	1.40E+09	6.97E+08	6.28E+10	6.53%	Skew Left
Damage F3	2.59E+07	1.29E+08	6.52E+07	5.71E+09	6.43%	Skew Left
Residence Time	1.08E+03	1.40E+03	1.40E+03	1.62E+03	0.13%	Bell Slight Left
Acceleraction	3.05E+07	6.06E+08	1.11E+08	9.00E+10	17.03%	Skew Left
Gradient of Accel	4.58E+19	7.98E+23	3.04E+20	5.68E+26	65.89%	Almost a Point
Stagnation Area	0.1091	0.1729	0.1461	0.6107	1.37%	Skew Left
Confluency	44.0896	1.58E+03	5.12E+02	2.90E+04	5.65%	Skew Left
Principal Shear Stress	9.20E+05	3.61E+06	2.05E+06	1.40E+08	5.47%	Skew Left
Elongation	1.05E+05	6.90E+05	3.50E+05	3.25E+07	6.53%	Skew Left
Peclet Number	6.71E+11	7.06E+11	7.06E+11	7.54E+11	0.06%	Normal
Damkohler Number	0.104	0.7794	0.5193	2.9824	2.22%	Skew Left
Platelet Stim. Funct.	3.09E+03	7.47E+03	6.73E+03	3.84E+04	1.43%	Skew Left

Functions, such as PL blood damage and Damkohler Number, that have a large gap between the mean and median also show skewed histograms. Table 5 shows the direction in which the value is skewed. The functions for Peclet Number and residence time both show histograms that are almost "normal" or Gaussian, which is why they have small variances.

The discrete optimums for the objective functions were also available through this study. All of the functions representing hemolysis or platelet activation had the same optimal point, except for the PSF. Since PSF is essentially the square root of the approximated power-law blood damage model, it should have the same optimal point. But, since time is inversely proportional to velocity, the factor epsilon had to be added to prevent a division by zero. This could be responsible for the slight mathematical variation in the functions. Residence time and stagnation area both shared their optimal point. Although most of the cannulae have different optimums, the functions representing clearance and recirculation tended toward narrow channels; while the hemolysis related function tend toward wider channels with low velocities. The acceleration channel tries to "square off" the turn.

3.2.2   Summary of the Statistical Analysis

Table 4 shows the correlation matrix for the design space using the integral norm approach. 1249 solutions were required to cover the entire space. The functions that have been linked to hemolysis did show high correlation with each other (C>0.95). The platelet stimulation function

also showed a reasonable correlation to the other power-law damage models (C>0.8). This was surprising since the PSF is approximately the square root of the hemolysis model. The correlation between the damage function using the maximum principal shear stress and the index based on viscous shear stress indicated that they were virtually equivalent. The acceleration force was found to correlate to the hemolysis models, but not as well as amongst each other (0.93>C>0.92 to >0.99). There were no anti-correlated functions (C<-0.75). This means that there are no one-to-one trade offs in the objective functions, so is possible to improve all of the objective functions to some extent. Peclet Number, stagnation area, confluence, and the Damkohler Number all appear to be independent of the each other and the other functions. The gradient of acceleration, although capable of determining jet flow, does not correlate with the various hemolysis models. This means that it is unlikely that this function actually contributes significantly to hemolysis.

The principal component analysis yielded eigenvalues that were ranked from the lowest to highest as shown in Figure 6. The cumulative percentages indicate that only three to four of the objective functions represent more than 90% of the overall information represented by the correlation matrix. It is statistically acceptable to use only four out of 15 for the optimization method. Although four functions should be used to reach 90% of the information, three should be sufficient, since the gradient of acceleration does not appear to correlate with hemolysis.

The correlation matrix for the infinity norm and the average norm were also evaluated. There were no strong correlations among the objective functions evaluated by the infinity norm, except for the PL models. They also showed little correlation to the equivalent function evaluated with the integral norm. This is most likely because these are evaluated at a single point in the flow field, where the integral and average norms are evaluated over the entire flow field. Integrals tend to smooth out noisy data. The correlation matrix for the average norm showed similarities to that of the integral norm. This is because the ratio between each function does not change with the norm.

More statistical information can be gathered from the design space study. Table 5 shows the minimum and maximum of the integral norm, the mean and medium of integral norm, and the variance of the design space. Almost all of the functions had a variance of 4-6% and several orders of magnitude difference between their max and min values. The only objective functions that had a lower variance were residence time (0.13%), stagnation area (1.37%), Peclet Number

(0.06%), Damkohler Number (2.22%), and the PSF (1.43%). The acceleration force and the gradient of acceleration both had high variances, 17.03% and 65.9% respectively.

Functions, such as PL blood damage and Damkohler Number, that have a large gap between the mean and median also show skewed histograms. Table 5 shows the direction in which the value is skewed. The functions for Peclet Number and residence time both show histograms that are almost "normal" or Gaussian, which is why they have small variances.

The discrete optimums for the objective functions were also available through this study. All of the functions representing hemolysis or platelet activation had the same optimal point, except for the PSF. Since PSF is essentially the square root of the approximated power-law blood damage model, it should have the same optimal point. But, since time is inversely proportional to velocity, the factor epsilon had to be added to prevent a division by zero. This could be responsible for the slight mathematical variation in the functions. Residence time and stagnation area both shared their optimal point. Although most of the cannulae have different optimums, the functions representing clearance and recirculation tended toward narrow channels; while the hemolysis related function tend toward wider channels with low velocities. The acceleration channel tries to "square off" the turn.

3.3   THE OPTIMIZED 2-D CANNULA

The single objective optimization was successful and can be seen in Figure 7. Most of the runs took only a few iterations (about 5-10) to reach a minimum. The exception was the damage function, which took an average 50 iterations to reach its minimum. Table 7 shows the optimization results and compared the different objective functions. The minimum-stagnation area cannula was very similar to the pinched cannula from the qualitative analysis. The maximum-Peclet Number cannula exhibited a constriction, but it was not as pronounced at the one in the minimum stagnation area cannula. The Peclet Number was found to vary by less than 10% between each design. Stagnation area was similar between the maximum-Peclet Number cannula, the minimum-confluence cannula, and the minimum-stagnation area cannula, but was almost 4 times as high in the minimum-viscous dissipation cannula. The hemolysis indicators increase as the cannula started to pinch off as expected.
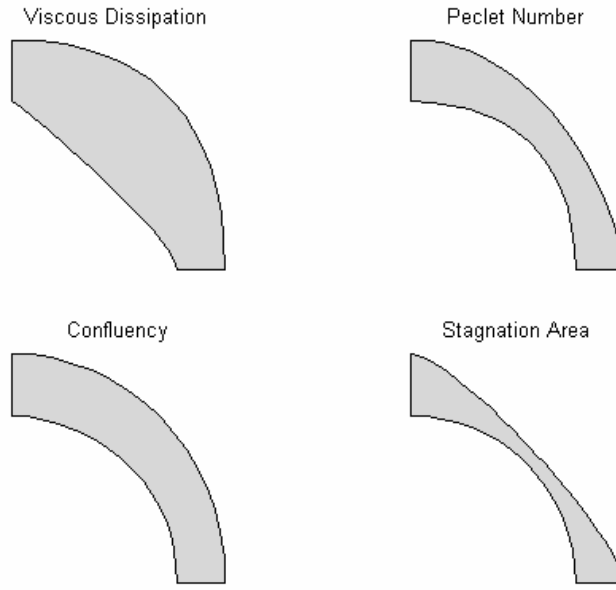
Viscous Dissipation

Peclet Number

Confluency

Stagnation Area

Figure 7: The optimal 2-D cannulas corresponding to various objective functions.

Table 6: Objective function values in each of the optimum cannula.

	Minimum Viscous Dissipation	Maximum Peclet Number	Minimum Confluence	Minimum Stagnation Area	MOO Cannula
Viscous Dissipation	2.41e5	1.10e6	4.39e5	1.315e7	1.24e6
Confluence	18,600	491	44	12,525	947
Peclet Number	7.23e11	7.29e11	7.27e11	7.16e11	7.26e11
Stagnation Area	0.5509	0.1650	0.1472	0.1213	0.1805
Damage Model	1.48e12	7.75e12	2.92e12	1.18e14	9.33e12

Figure 8 shows that the MOO cannula using the Koski transformation was also slightly pinched. This means that the Peclet Number dominated the Koski transformation. The viscous dissipation and PL blood damage model increased by just under an order of magnitude over the SOO optimal point, while the confluence rose by almost 2 orders of magnitude. There was only a

50% increase in the value for the stagnation area, and slightly less than a half percent change in the Peclet Number.
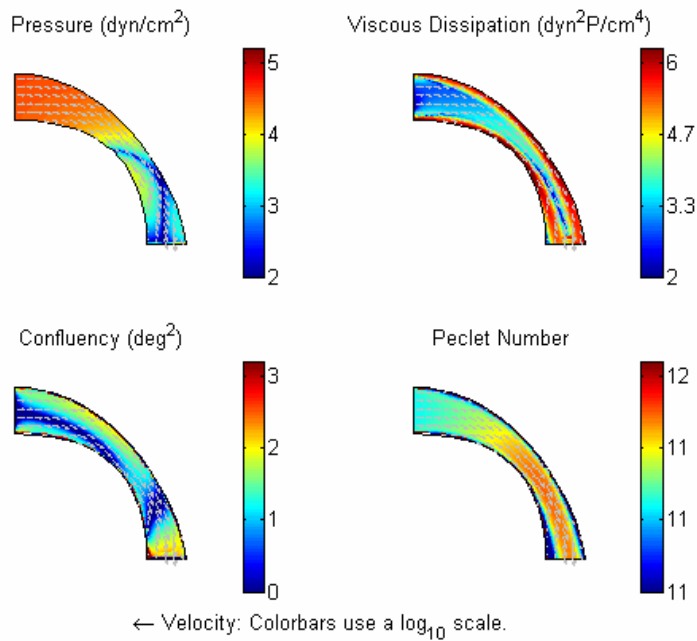
Figure 8: The objective functions of the multi-objective optimized cannula.

Figure 9 shows the MOO cannula using the KS transformation. This cannula seems to an improvement over the other designs. The viscous dissipation, PL damage model, and confluence increased by only 50%, as compared to 400%, 500%, and 20000% using the KS transformation. There was almost no change in the Peclet number between the two MOO cannulas. The stagnation area increased by 14.6% when using the second method. It should be noted that the KS transform does not normalize by the variance of the individual functions, which may allow a function with the greatest variance to dominate the MOF. Since both confluency and the shear damage functions increase rapidly when a constriction is developed, these functions tended to force the geometry toward a straighter configuration.
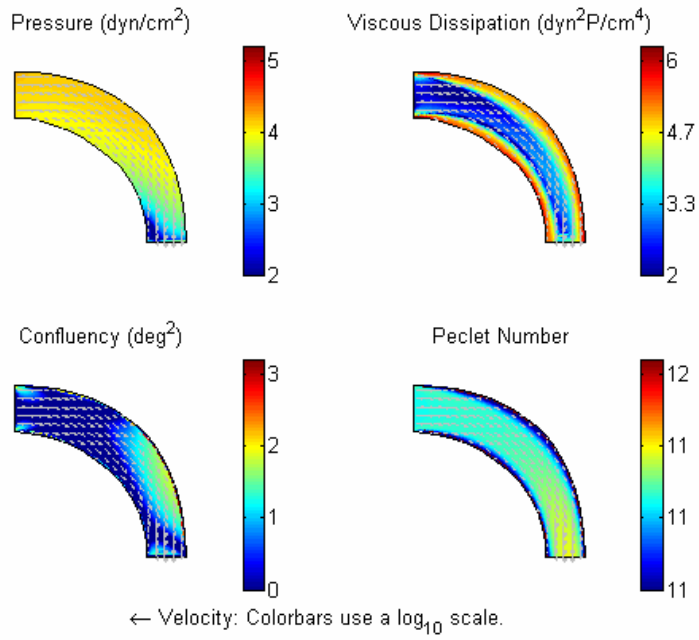
Figure 9: Second set of multi-objective optimized (MOO) cannulae.

4.0   DISCUSSION AND CONLUSIONS

There are numerous possible choices for objective functions that represent blood damage. Viscous dissipation, confluency, stagnation area, and Peclet Number were all shown to have great promise in observing blood damage in its various forms. They were selected above the rest because they had better qualities than the other function. Viscous dissipation had a reasonable resemblance to the power-law blood damage models for shear induced hemolysis and platelet activation, but showed better mathematical behavior. *Confluency*, which is somewhat difficult to define, was very effective at penalizing designs with recirculation regions. Recirculation is typically linked with high shear rates and buildup of platelet agonist and coagulation factors. *Stagnation area* is a distant second to confluency, if an unacceptable reference flow field cannot be found. It has a decent variance over the design space, but cannot be used to penalize recirculation zones that have high velocities. *Peclet Number* is a good index for representing the clearance of agonists, coagulation factors, and active platelets. It suffers from a small variance in the design space, but also serves to balance the behavior of viscous dissipation. All three objective functions exhibited robust performance about their optimal points, and are therefore good selections.

This study illustrates the crucial importance of multi-objective optimization for designing blood-wetted medical devices, because the mechanism for various forms of blood damage compete with one another. For example, shear, which is a measure of hemolysis and platelet activation, competes with convection, which is a measure of agonist build up, platelet adhesion, and the build up of coagulation factors. Unfortunately, multi-objective optimization is still in its infancy and an ideal approach has not been fully developed. Currently, two popular and systematic methods were used based on normalizing the objective functions and do show reasonable results.

4.1 QUALITATIVE ANALYSIS OF OBJECTIVE FUNCTIONS

The qualitative analysis gave great insight into the ability of several functions to evaluate blood damage. Several objective functions showed very similar patterns in the flow field, which would indicate that they are correlated with one another. The total area of the design was shown to contribute to the optimal point. This type of analysis extends beyond optimization and is suitable for analyzing CFD results in general. This allows for different design options or devices to be compared, using the user preferred CFD package.

This analysis also gives preliminary guidance into which objectives are appropriate for optimization. It is obvious that confluency is the only objective function that properly defines recirculation regions in an Eulerian frame of reference. The Peclet Number also provides a good indicator for the clearance in a device. The various functions that relate to shear induced hemolysis and platelet activation show similar features. This tends to indicate that they are interchangeable and that there is no preference in using one over the other, but further analysis is necessary in order to show that this correlation exists.

4.2 QUANTITATIVE ANALYSIS OF OBJECTIVE FUNCTIONS

A more mathematical analysis of the objective function validated some of the results from the qualitative analysis, but also gave more insight into the behavior of the objective functions. The blood damage models have been reduced to viscous dissipation, or elongation in the principal frame, the confluency or stagnation area, and Peclet Number. These functions are not correlated with each other and provide a good basis for multi-objective optimization.

Several objective functions were eliminated out of mathematical preference, first through logical deduction and secondly by examining their Hessian matrix. The first function that was eliminated was vorticity since it only correlates to shear stress (a known cause of hemolysis) but does not have its own mechanism for destroying blood cells. Unlike viscous dissipation and shear stress, which are linked to blood damage through mechanistic means, flows with high shear, especially turbulent flow, generally have high vorticity, but vorticity can occur where there is no shear. Blackshear suggests that turbulent eddies on the scale of the RBC cause

hemolysis, but the means of damage is not clear. The second problem with this reasoning is that our current modes of simulation cannot simulate eddies of this size. But, consider solid body rotation of a fluid with the same density of a red blood cell. This is a flow that has vorticity (twice the rotational rate) but no shear stress. Logically, one would expect that there would be no hemolysis in the solid body rotation since there is no deformation of the cells. The work of Sutera et al. (33) seems to support this hypothesis. They measured the effect of turbulence on hemolysis, and showed that free turbulence did not raise the level of hemolysis. The turbulence does increase hemolysis when in the presence of a wall because it increases the shear stress at the wall. Currently we are discussing several experiments in order to investigate this hypothesis, but for now it will be dropped until further study can be made.

The second function that should be dropped is the elongation. Elongation is commonly used in chemical engineering for studying polymer flows. As mention above, it is the RMS value of the normal components of the strain rate tensor, D. There is a debate as to what frame of reference should be used to determine the elongation of a cell. Four frames are important to consider. The first is the Eulerian fixed frame, which simplifies the problem considerable since no transformations are necessary to calculate the function. The second frame is the local flow frame, where the elongation is calculated along the streamline. This is how polymers usually align themselves in the flow field. Thirdly, there is the principal frame where the elongation should be at its maximum. The forth is based off of experimental results.

Normally, we would expect the greatest deformation in the principal axis, but this is not what is seen experimentally. For Couette flow, the principal axis is aligned at 45° but experimental results show that the red blood cells align at approximately 20° with some variance due to flow and hematocrit. This would indicate that the frame should be rotated 20° for Couette flow, but it the angle of alignment is different for various flows. There is thus a large uncertainty as to the frame in which elongation should be calculated. In the principal frame elongation becomes the strain rate, meaning that ε^2 is proportional to viscous dissipation. All the analysis for viscous dissipation would then hold for principal elongation.

The second variations of select objective functions were evaluated for positive definiteness in order to further reduce the number of objective functions. Normally, the second variation would require the solution of the sensitivity of the PDE to the design parameter, but

this value is independent of the objective functions, so we will only worry about the behavior of the objective functions themselves.

The convergence of an objective function is directly tied to its Hessian matrix. If the matrix is positive definite, then the convergence to a minima is guaranteed and should be relatively fast. If the matrix is not positive definite, then the optimization routine can be attracted to a saddle point or a maximum. Convergence for functions that do not have positive definite Hessians depends on the nearness of the guess to the initial point. The Hessian is related to the second variation of the objective function found using calculus of variations. Variations were calculated for viscous dissipation, the power-law blood damage models, residence time, and Peclet Number (Table 7). The symbol "^" implies the first variation, while the symbol "~" implies the second variation of the function. The second variation of the residence time and that of the power-law damage functions have negative components, which indicate that the Hessian may not be positive definite at all points. The second variations of viscous dissipation and the Peclet Number are always positive definite which make them suitable for optimization.

Table 7: First and second variations of selected objective functions.

Function	Variation Order	Variational Form
Viscous Dissipation	1ˢᵗ	$2\mu\int_{\Omega}\left(2u_x\hat{u}_x + (u_y + v_x)(\hat{u}_y + \hat{v}_x) + 2v_y\hat{v}_y\right)d\Omega$
	2ⁿᵈ	$2\mu\int_{\Omega}\left(2\tilde{u}_x\hat{u}_x + (\tilde{u}_y + \tilde{v}_x)(\hat{u}_y + \hat{v}_x) + 2\tilde{v}_y\hat{v}_y\right)d\Omega$
PL Blood Damage Model	1ˢᵗ	$\int_{\Omega}\left(\dfrac{\mu\hat{C}_{VD}}{U} - \dfrac{\mu C_{VD}}{U^3}\left(u\hat{u} + v\hat{v}\right)\right)d\Omega$
	2ⁿᵈ	$\int_{\Omega}\left(\dfrac{\mu\tilde{C}_{VD}}{U} - \dfrac{\mu\hat{C}_{VD}}{U^3}\left(u\hat{u} + v\hat{v}\right)\right)d\Omega$ $+ \int_{\Omega}\left(\dfrac{3\mu C_{VD}}{2U^5}\left(u\hat{u} + v\hat{v}\right)\left(u\tilde{u} + v\hat{v}\right)\right)d\Omega$ $- \int_{\Omega}\left(\dfrac{\mu\hat{C}_{VD}}{U^3}\left(\tilde{u}\hat{u} + \tilde{v}\hat{v}\right)\right)d\Omega$
Residence Time	1ˢᵗ	$-\int_{\Omega}\left(\dfrac{u\hat{u} + v\hat{v}}{U^3}\right)d\Omega$
	2ⁿᵈ	$-\int_{\Omega}\left(\dfrac{\tilde{u}\hat{u} + \tilde{v}\hat{v}}{U^3} - \dfrac{3}{2}\dfrac{u\hat{u} + v\hat{v}}{U^5}\left(u\tilde{u} + v\tilde{v}\right)\right)d\Omega$
Peclet Number	1ˢᵗ	$\int_{\Omega}\left(\dfrac{2(u\hat{u} + v\hat{v})d^2}{D^2}\right)d\Omega$
	2ⁿᵈ	$\int_{\Omega}\left(\dfrac{2(\tilde{u}\hat{u} + \tilde{v}\hat{v})d^2}{D^2}\right)d\Omega$

4.3   OPTIMIZATION OF A 2-D CANNULA

There were several interesting results from this study. The first is that the power-law objective function did indeed behave poorly, just as predicted by the mathematical analysis. Approximation methods, like the Picard Method, must be used if the power-law models are to be implemented. This means that the user must use more advanced optimization techniques, and cannot use the common canned methods. The other option is to use viscous dissipation. The two did reach the same optimal point, and no special method would be required for the convergence. The optimal shapes for these types of functions were used in section 4, and shows that the damage function is dominated by the shear stress. Since the flow is low enough, the stress caused by the recirculation zone is not large enough to impact the value of the objective function. The cannula increased its size in order to reduce the flow rate and the resulting stresses, until it reached the pre-described limits of the shape (6.2). It is possible that there is a point, where flow rate decreased enough to where the velocity term would dominate, but the constraints prevented this.

The Peclet Number was optimized and the cannula appeared to have a slight constriction in its side. The size of the cannula decreases in order to increase the flow speed through the cannula. This makes sense, since the Peclet number is the balance of convection to diffusion. The cannula must increase the velocity, since the diffusion term is constant. The value seems to reach a balance at the point where flow would start to separate and cause a low velocity recirculation region at the distal end.

The cannula generated by the *confluence* objective function was nearly circular, and if weighted Bezier curves had been used to describe the geometry, it would probably be completely circular. This again makes sense because the desired flow angle was selected to a circular path. This however implies that the use of the confluency objective is fairly limited to the user's a-priori definition of the desired flow path. In some circumstances this would be desirable; however for complex flow, it would be more advantageous to use the Stokes flow solution (low Reynolds Number) to prescribe the desired path. Stokes flows are dominated by viscosity, as opposed to momentum, and will typically not exhibit recirculation zones. Any recirculation zones that appear at higher Reynolds numbers will show a significant deviation from the Stokes flow. This method also solves the problem of more complex geometries.

This thesis has lead to a novel and innovative design of ventricular cannula that shows numerical improvements over the previous design. The cannula has a larger upper portion, which tapers down as it approaches the device. This reduces shear, since the initial flow is lower. It also reduces the "sloshing" of blood toward the outer portion of the pipe. This phenomenon is momentum related, and is reduced by having a lower momentum going into the turn. This also decreases the high shear stress that forms when the fluid from the central core contacts the outer wall. Finally, this design reduces the strength of the Dean vortices, which improves the blood damage as well as the efficiency of the VAD to which it is connected. The new cannula then tapers, causing the flow to accelerate. This increases the shear rate, but also increases the convection of the undesirable chemicals and platelets. Another important result is that the velocity profile is more uniform than the previous one. This also helps to improve the efficiency of the VAD.

5.0   FUTURE WORK

This thesis had two goals. The first was to advance the understanding of current methods for relating CFD results to blood damage. The objective functions that were chosen represent either common methods of determining blood damage or other functions that seem to fit well with concepts of blood damage. Although this list was comprehensive there are certainly other methods that could be examined. It is also desirable to combine CFD with other simulation techniques, such as the convection-diffusion (C-D) equation, which could be used to explicitly compute clearance (wash out.) Even more complex than the C-D equation are various models of platelet aggregation. Another area of future work also includes modeling actual blood cell rupture. Finally, the power-law blood damage models can be evaluated in a Lagrangian frame of reference. All three of these areas require more work in order to have a better understanding of blood damage on both a macroscopic and microscopic level.

Besides examining new methods for describing blood damage, the current models were only examined in a simple 2-D flow. More work should be done in order to compare these objectives in more complex flows, for example through a blade path of a ventricular assist device, or in 3D flow cases. For this thesis, it was assumed that the results would be the same as in the 3D case. Verification would still be necessary to prove this hypothesis. Other variations that must be analyzed involve other flow equations, such as turbulent flow, non-Newtonian flow, and visco-elastic flows.

Future continuation of this research should also consider the use of more robust methods of optimization. The description of the geometry, for example should be refined to minimize the curvature and thus be less sensitive to errors in manufacturing or other factors that were not taken into account in simulation or optimization routine. These factors can include changes in viscosity or other alteration in the blood flow, defects in cannula, and changes caused by implantation.

The second goal of this thesis was to improve the design of a specific flow path, representative of a ventricular cannula. The new cannula resulting from this optimization exercise would benefit from experimental validation for its superiority to be definitively convincing. This will help verify that the selected objective functions are acceptable, and more importantly demonstrate that there is significant room for improvement in the design of cannula.

Future extension of this research should also consider the design over a range of operating conditions. Flow in the cardiovascular system is not constant and should be taken into account in the optimization routine. Several methods could be used, including pulsatile flow and optimization in unsteady flow. This is very difficult and computationally expensive, and still assumes a flow regime that might not be ideal. Another method that could possibly help deal with this is to run multi-objective optimization of a range of flow conditions with, but weight the desired flow regime higher than the outliers. VADs sometime allow for the heart of the patient to recover, in which case the patient is weaned off of the device. This means that the Cannula and VADs must be designed to operate at lower flow rates than normal to accommodate weaning of patients. This can likewise be accommodated with a time varying flow that is either ramped up to nominal or vice versa, or by using a weighted function over the flow regime.

Finally, the optimal design of the cannula tip is important. Carefully consideration must be taken to account for the heart-cannula interaction. Thrombosis commonly occurs at the area where the cannula is placed into the heart. Another challenge is that the blood can be damaged at the entrance to the cannula, so hemolysis could potentially be decreased by shape optimization. Also, the exact placement of the cannula within the ventricle is impossible since it is not possible to see inside the ventricle during implantation and each heart is unique. Multi-objective optimization could also be implemented to reduce the effects of less than ideal placement using similar weighting methods as described above.

BIBLIOGRAPHY

1. Giersiepen M, Wurzinger LJ, Opitz R, Reul H. Estimation of shear stress-related blood damage in heart valve prostheses--in vitro comparison of 25 aortic valves. Int J Artif Organs 1990;13(5):300-6.

2. James NL, Wilkinson CM, Lingard NL, van der Meer AL, Woodard JC. Evaluation of hemolysis in the VentrAssist implantable rotary blood pump. Artif Organs 2003;27(1):108-13.

3. Grigioni M, Daniele C, Morbiducci U, D'Avenio G, Di Benedetto G, Barbaro V. The power-law mathematical model for blood damage prediction: analytical developments and physical inconsistencies. Artif Organs 2004;28(5):467-75.

4. Sorensen EN, Burgreen GW, Wagner WR, Antaki JF. Computational simulation of platelet deposition and activation: I. Model development and properties. Ann Biomed Eng 1999;27(4):436-48.

5. Sorensen EN, Burgreen GW, Wagner WR, Antaki JF. Computational simulation of platelet deposition and activation: II. Results for Poiseuille flow over collagen. Ann Biomed Eng 1999;27(4):449-58.

6. Ogino H, Klangsuk N, Jin W, Bowles CT, Yacoub MH. Influence of the compliance of the pump housing and cannulas of a paracorporeal pneumatic ventricular assist device on transient pressure characteristics. Artif Organs 1995;19(6):525-34.

7. Ogino K, Hisatome I, Kotake H, Furuse T, Mashiba H, Kuroda H, et al. A case of four coronary artery fistulae originating from three vessels associated with aneurysm. Eur Heart J 1987;8(11):1260-3.

8. Richenbacher WE, Marks JD. Cannula selection and cannulation techniques for nonpulsatile mechanical ventricular assistance. Artif Organs 1995;19(6):519-24.

9. Deleuze P, Okude J, Leandri J, Rey P, Loisance D. An original inflow cannula for paracorporeal assist devices. ASAIO Trans 1989;35(3):442-4.

10. Curtis AS. A Multiple Modality Study of the Hemodynamics of Left Ventricular Cannulation [Masters of Science in Biomedical Engineering]. Pittsburgh: University of Pittsburgh; 1998.

11. He B. Shape Optimization of Navier-Stokes Flow with Application to Design of Artificial Heart Components [Ph.D]. Pittsburgh: Carnegie Mellon University; 1996.

12. Antaki JF, Dennis TJ, Konishi H, Brown ME, Maher TR, Tomczak JP, et al. An improved left ventricular cannula for chronic dynamic blood pump support. Artif Organs 1995;19(7):671-5.

13. Hanson SR. Device Thrombosis and Thromboembolism. Cardiovasc. Pathol. 1993;2:157S-165S.

14. Guyton AC, Hall JE. Textbook of medical physiology. 10th ed. Philadelphia: Saunders; 2000.

15. Saladin KS. Anatomy & physiology: the unity of form and function. 2nd ed. Boston: McGraw-Hill; 2000.

16. Chien S, Usami S, Taylor HM, Lundberg JL, Gregersen MI. Effects of hematocrit and plasma proteins on human blood rheology at low shear rates. J Appl Physiol 1966;21(1):81-7.

17. Paut O, Bissonnette B. Effects of temperature and haematocrit on the relationships between blood flow velocity and blood flow in a vessel of fixed diameter. Br J Anaesth 2002;88(2):277-9.

18. Walburn FJ, Schneck DJ. A constitutive equation for whole human blood. Biorheology 1976;13(3):201-10.

19. Thurston GB. Viscoelasticity of human blood. Biophys J 1972;12(9):1205-17.

20. Deutsch S, Phillips WM. An interpretation of low strain rate blood viscosity measurements: a continuum approach. Biorheology 1976;13(5):297-307.

21. Sharp MK, Thurston GB, Moore JE, Jr. The effect of blood viscoelasticity on pulsatile flow in stationary and axially moving tubes. Biorheology 1996;33(3):185-208.

22. Mann DE, Tarbell JM. Flow of non-Newtonian blood analog fluids in rigid curved and straight artery models. Biorheology 1990;27(5):711-33.

23. Mann KA, Deutsch S, Tarbell JM, Geselowitz DB, Rosenberg G, Pierce WS. An experimental study of Newtonian and non-Newtonian flow dynamics in a ventricular assist device. J Biomech Eng 1987;109(2):139-47.

24. Mizuno T, Tsukiya T, Taenaka Y, Tatsumi E, Nishinaka T, Ohnishi H, et al. Ultrastructural alterations in red blood cell membranes exposed to shear stress. Asaio J 2002;48(6):668-70.

25. Blackshear PL, Jr., Dorman FD, Steinbach JH. Some Mechanical Effects That Influence Hemolysis. Trans Am Soc Artif Intern Organs 1965;11:112-7.

26. Blackshear PL, Jr., Dorman FD, Steinbach JH, Maybach EJ, Singh A, Collingham RE. Shear, wall interaction and hemolysis. Trans Am Soc Artif Intern Organs 1966;12:113 20.

27. Bernstein EF, Blackshear PL, Jr., Keller KH. Factors influencing erythrocyte destruction in artificial organs. Am J Surg 1967;114(1):126-38.

28. Blackshear PL, Jr., Forstrom RJ, Dorman FD, Voss GO. Effect of flow on cells near walls. Fed Proc 1971;30(5):1600-11.

29. Reul H, Talukder N, Muller EW. Fluid mechanics of the natural mitral valve. J Biomech 1981;14(5):361-72.

30. Wurzinger LJ, Opitz, R., Eckstein, H. Mechanical Blood Trauma. Angeilogie 1986;38(3):81-97.

31. Umezu M, Fujimasu, H., Yamada, T., Fijimoto, T., Ranakawake, M., Nogawa, A., and Kijima T. Fluid Dynamic Investigation of Mechanical Blood Hemolysis. Heart Replacement: The 5th International Symposium on Artificial Heart and Assist Devices 1995;5:327-335.

32. Kingsbury C, Kafesjian R, Guo G, Adlparvar P, Unger J, Quijano RC, et al. Cavitation threshold with respect to dP/dt: evaluation in 29 mm bileaflet, pyrolitic carbon heart valves. Int J Artif Organs 1993;16(7):515-20.

33. Sutera SP, Croce PA, Mehrjardi M. Hemolysis and subhemolytic alterations of human RBC induced by turbulent shear flow. Trans Am Soc Artif Intern Organs 1972;18(0):335-41, 347.

34. Sutera SP, Mehrjardi MH. Deformation and fragmentation of human red blood cells in turbulent shear flow. Biophys J 1975;15(1):1-10.

35. Jaenike JR. The renal lesion associated with hemoglobinemia. I. Its production and functional evolution in the rat. J Exp Med 1966;123(3):523-35.

36. Jaenike JR, Schneeberger EE. The renal lesion associated with hemoglobinemia. II. Its structural characteristics in the rat. J Exp Med 1966;123(3):537-45.

37. Jaenike JR. The renal lesion associated with hemoglobinemia: a study of the pathogenesis of the excretory defect in the rat. J Clin Invest 1967;46(3):378-87.

38. Abrams C, and Lawrence, F.B. Platelet Signal Transduction. In: Coleman RW, Hirsh, J., Marder, V.J., Clowes, A.W., and George, J.N., editor. Hemostasis and Thrombosis: Basic Principles & Clinical Practice. 4th ed: Lippincott, Williams, and Wilkins; 2001. p. 541-559.

39. Tandon P, Diamond SL. Hydrodynamic effects and receptor interactions of platelets and their aggregates in linear shear flow. Biophys J 1997;73(5):2819-35.

40.	Hanson SR, and Harker, L.A. Blood Coagulation and Blood-Material Interactions. Biomaterials Science 1996:193-198.

41.	Mushahwar SS, Pyatt JR, Lowe R, Morrison WL, Perry RA, Ramsdale DR. Clinical outcomes of long coronary stents: a single-center experience. Int J Cardiovasc Intervent 2001;4(1):29-33.

42.	Manolis AS, Chiladakis J, Hahalis G, Agelopoulos G. Initial experience with a newer generation coronary stent. J Invasive Cardiol 2001;13(3):217-22.

43.	Holmes DR, Jr. In-stent restenosis. Rev Cardiovasc Med 2001;2(3):115-9.

44.	Chuter TA. Stent-graft design: the good, the bad and the ugly. Cardiovasc Surg 2002;10(1):7-13.

45.	Keiser JA, Uprichard AC. Restenosis: is there a pharmacologic fix in the pipeline? Adv Pharmacol 1997;39:313-51.

46.	Sigwart U. Coronary stents. Z Kardiol 1995;84 Suppl 2:65-77.

47.	Klugherz BD, Herrmann HC. Mechanical Prosthetic Valve Thrombosis: Case Report and Review of the Literature. J Thromb Thrombolysis 1998;6(3):253-259.

48.	Vongpatanasin W, Hillis LD, Lange RA. Prosthetic heart valves. N Engl J Med 1996;335(6):407-16.

49.	Antunes MJ. Reoperations on cardiac valves. J Heart Valve Dis 1992;1(1):15-28.

50.	Metzdorff MT, Grunkemeier GL, Pinson CW, Starr A. Thrombosis of mechanical cardiac valves: a qualitative comparison of the silastic ball valve and the tilting disc valve. J Am Coll Cardiol 1984;4(1):50-3.

51.	Kloster FE. Diagnosis and management of complications of prosthetic heart valves. Am J Cardiol 1975;35(6):872-85.

52.	Hylen JC. Mechanical malfunction and thrombosis of prosthetic heart valves. Am J Cardiol 1972;30(4):396-404.

53.	Wagner WR, Schaub RD, Sorensen EN, Snyder TA, Wilhelm CR, Winowich S, et al. Blood biocompatibility analysis in the setting of ventricular assist devices. J Biomater Sci Polym Ed 2000;11(11):1239-59.

54.	Kasirajan V, McCarthy PM, Hoercher KJ, Starling RC, Young JB, Banbury MK, et al. Clinical experience with long-term use of implantable left ventricular assist devices: indications, implantation, and outcomes. Semin Thorac Cardiovasc Surg 2000;12(3):229-37.

55.	1997;62 Suppl 1.

56.   Schwab SJ. Assessing the adequacy of vascular access and its relationship to patient outcome. Am J Kidney Dis 1994;24(2):316-20.

57.   Albers FJ. Causes of hemodialysis access failure. Adv Ren Replace Ther 1994;1(2):107-18.

58.   Haimov M. Vascular access for hemodialysis. Surg Gynecol Obstet 1975;141(4):619-25.

59.   Bordenave L, Remy-Zolghadri M, Fernandez P, Bareille R, Midy D. Clinical performance of vascular grafts lined with endothelial cells. Endothelium 1999;6(4):267-75.

60.   Callow AD. Problems in the construction of a small diameter graft. Int Angiol 1988;7(3):246-53.

61.   Ritter EF, Kim YB, Reischl HP, Serafin D, Rudner AM, Klitzman B. Heparin coating of vascular prostheses reduces thromboemboli. Surgery 1997;122(5):888-92.

62.   Burkel WE. The challenge of small diameter vascular grafts. Med Prog Technol 1988;14(3-4):165-75.

63.   Antaki JF, Ghattas O, Burgreen GW, He B. Computational flow optimization of rotary blood pump components. Artif Organs 1995;19(7):608-15.

64.   Jones SA. A relationship between Reynolds stresses and viscous dissipation: implications to red cell damage. Ann Biomed Eng 1995;23(1):21-8.

65.   Sutera SP. Flow-induced trauma to blood cells. Circ Res 1977;41(1):2-8.

66.   Yeleswarapu KK, Antaki JF, Kameneva MV, Rajagopal KR. A mathematical model for shear-induced hemolysis. Artif Organs 1995;19(7):576-82.

67.   Mitamura Y, Nakamura, H., and Sekine, K. Prediction of Hemolysis in Rotary Blood Pumps with Computational Fluid Dynamics Analysis. J. Congestive Heart Failure Circulatory Support 2000;1(4):331-336.

68.   Wootton DM, Ku DN. Fluid mechanics of vascular systems, diseases, and thrombosis. Annu Rev Biomed Eng 1999;1:299-329.

69.   Jesty J, Yin W, Perrotta P, Bluestein D. Platelet activation in a circulating flow loop: combined effects of shear stress and exposure time. Platelets 2003;14(3):143-9.

70.   Tambasco M, Steinman DA. On assessing the quality of particle tracking through computational fluid dynamic models. J Biomech Eng 2002;124(2):166-75.

71.   Joseph D. Interrogation of Direct Numerical Simulation of Solid-Liquid Flow. Minneapolis: University of Minneapolis; 2002.

72. Ghattas O, and Malcevic, I. Dynamic-Mesh Finite Element Method for Lagrangian Computational Fluid Dynamics. Finite Elements in Analysis and Design 2002;38.

73. Cardoze D, Cunha, A., Miller, G., Phillips, T., and Walkington N. A Bezier Approach to Unstructured Moving Meshes. Proceedings of the 20th Symposium on Computation Geometry 2004.

74. Burgreen GW, Antaki JF, Wu J, le Blanc P, Butler KC. A computational and experimental comparison of two outlet stators for the Nimbus LVAD. Left ventricular assist device. Asaio J 1999;45(4):328-33.

75. Chaubal CV, and Leal, L.G. Smoothed Particle Hydrodynamic Techniques for the Solution of Kinetic Theory Problems: Part 2. The effect of flow perturbations on the simplle shear behaviot of LCPs. J. Non-Newtonian Fluid Mech. 1999;82:25-55.

76. Goldsmith HL, Karino T. Platelets in a region of disturbed flow. Trans Am Soc Artif Intern Organs 1977;23:632-8.

77. Karino T, Goldsmith HL. Aggregation of human platelets in an annular vortex distal to a tubular expansion. Microvasc Res 1979;17(3 Pt 1):217-37.

78. Karino T, Goldsmith HL. Disturbed flow in models of branching vessels. Trans Am Soc Artif Intern Organs 1980;26:500-6.

79. Burgreen GW, Antaki JF, Griffith BP. A design improvement strategy for axial blood pumps using computational fluid dynamics. Asaio J 1996;42(5):M354-60.

80. Osher S, Fedkiw RP. Level set methods and dynamic implicit surfaces. New York: Springer; 2003.

81. Fogelson AL. Continuum models of Platelet Aggregation: Formulation and Mechanical Properties. SIAM J. Appl. Math 1992;52:1089-1110.

82. Gunzburger MD. Finite element methods for viscous incompressible flows: a guide to theory, practice, and algorithms. Boston: Academic Press; 1989.

83. Johnson C. Numerical Solution of Partial Differential Equations by Finite Elements Method: Cambridge University Prss; 1990.

84. Hansbo P, and Szepessy, A. A Velocity-Pressure Streamline Diffusion Finite Element Method for the Incompressible Navier-Stokes Equations. Computational Methods in Applied Mechanics and Engineering 1990;84:175-192.

85. Hughes T, Franca, L., and Hulbert, G. A New Finite Element Formulation for Computational Fluid Dynamics: Viii the Galerkin/Least-Squares Method for Advection-Diffusion Equations. Computational Methods in Applied Mechanics and Engineering 1989;73:173-189.

86.   Behr MaT, T. Finite Element Solution Strategies for Large-Scale Flow Simulations. Computational Methods in Applied Mechanics and Engineering 1994;112:3-24.

87.   Hughes T, Liu, W., and Brooks, A. Finite Element Analysis of Incompressible Viscous Flows by the Penalty Function Formulation. Journal of Computional Physics 1979;30:1-60.

88.   Codina R. An Iterative Penalty Method for the Finite Element Solution of Stationary Navier-Stokes Equations. Computational Methods in Applied Mechanics and Engineering 1993;110:237-262.

89.   Mizukami A. Element-by-Element Penalty / Uzawa Formulation for Large Scale Flow Problems. Computational Methods in Applied Mechanics and Engineering 1994;112:283-289.

90.   Fletcher R. Practical Methods of Optimization: John Wiley and Sons.; 1980.

91.   Gill PE, Murray, W., and Wright, M.H. Practical Optimization. London: Academic Press; 1981.

92.   Hoffman JD. Numerical methods for engineers and scientists. 2nd ed. New York: Marcel Dekker; 2001.

93.   Broyden CG. The Convergence of a Class of Doupe-rank Minimization Algorithms. J. Inst. maths. Applics. 1970;6:76-90.

94.   Fletcher R. A New Approach to Variable Metric Algorithms. Computer Journal 1970;13:317-322.

95.   Goldfarb D. A Family of Variable Metric Updates Derived by Variational Means. Mathematics of Computing 1970;24:23-26.

96.   Shanno DF. Conditioning of Quasi-Newton Methods for Function Minimization. Mathematics of Computing 1970;24(647-656).

97.   Fletcher R, and Powell, M.J.D. A Rapidly Convergent Descent Method for Minimization. Computer Journal 1963;6:163-168.

98.   Davidson WC. Variable Metric Method for Minimization. A.E.C. Research and Development Report 1959;ANL-5990.

99.   Schittowski K. NLQPL: A FORTRAN-Subroutine Solving Constrained Nonlinear Programming Problems. Annals of Operations Research 1985;5:485-500.

100.   Powell MJD. A Fast Algorithm for Nonlinearly Constrained Optimization Calculations. In: Watson GA, editor. Numerical Analysis: Springer Verlag; 1978.

101. Han SP. A Globally Convergent Method for Linear Programming. J. Optimization Theory and Applications 1977;22:297.

102. Biggs MC. Constrained Minimization Using Recursive Quadratic Programming. In: Dixon LCW, and Szergo, G.P., editor. Towards Global Optmization: North-Holland; 1975. p. 341-349.

103. Da Cunha NO, and Polak, E. Constrained Minimization Under Vector-valued Criteria in Finite Dimensional Spaces. j. Math. Anal. Appl. 1967;19:103-124.

104. Censor Y. Pareto Optimality in Multiobjective Problems. Appl. Math. Optimiz. 1977;4:41-59.

105. Marler RT, and Arora, J.S. Survey of Multi-Objective Optimization Methods for Engineering. Struct Multidisc Optim 2004;26:369-395.

106. Koski J, and Silvernnoinen, R. Norm Methods and Partial Weighting in Multicriterion Optimization of Structures. Int. J. Numer. Methods Eng. 1987;24:1101-1121.

107. Koski J. Multicriterion Optimization in Structural Design. In: Atrek E, Gallegher, R.H., Ragsdell, K.M., Zienkiewicz, O.C., editor. New Directions in Optimum Structural Design. New York: John Wiley and Sons; 1984. p. 483-503.

108. Kolesov VI, Levin AO, Vinogradov AG, Danilova LD. [on Changes of Morphological and Functional Properties of the Blood and Hemodynamics During the Use of the Niiekhaii (Aik-59) and Baliuzek's (Isl-2) Artificial Circulation Apparatus]. Grudn Khir 1963;49:34-40.

109. Smithwick W, 3rd, Kouchoukos NT, Karp RB, Pacifico AD, Kirklin JW. Late stenosis of Starr-Edwards cloth-covered prostheses. Ann Thorac Surg 1975;20(3):249-55.

110. Anzai N, Iriyama T, Yamada M, Ishihara S. Intravascular hemolysis with pulmonic stenosis. Occurrence after correction of subpulmonary ventricular septal defect. Chest 1977;71(4):561.

111. Solanki DL, Sheikh MU. Fragmentation hemolysis in idiopathic hypertrophic subaortic stenosis. South Med J 1978;71(5):599-601.